Catenin α 1 mutations cause familial exudative vitreoretinopathy by overactivating Norrin/β-catenin signaling

Xianjun Zhu,[1,2,3] Mu Yang,[1,2] Peiquan Zhao,[4] Shujin Li,[1,2] Lin Zhang,[1] Lulin Huang,[1] Yi Huang,[1] Ping Fei,[4] Yeming Yang,[1] Shanshan Zhang,[1] Huijuan Xu,[1] Ye Yuan,[1] Xiang Zhang,[4] Xiong Zhu,[1] Shi Ma,[1] Fang Hao,[1] Periasamy Sundaresan,[5] Weiquan Zhu,[6] and Zhenglin Yang[1,2,3]

[1]Sichuan Provincial Key Laboratory for Human Disease Gene Study, Sichuan Provincial People's Hospital, University of Electronic Science and Technology of China, Chengdu, Sichuan, China. [2]Research Unit for Blindness Prevention of the Chinese Academy of Medical Sciences (2019RU026), Sichuan Academy of Medical Sciences and Sichuan Provincial People's Hospital, Chengdu, Sichuan, China. [3]Chinese Academy of Sciences Sichuan Translational Medicine Research Hospital, Chengdu, China. [4]Department of Ophthalmology, Xinhua Hospital, School of Medicine, Shanghai Jiaotong University, Shanghai, China. [5]Department of Genetics, Aravind Medical Research Foundation, Aravind Eye Hospital, Madurai, Tamil Nadu, India. [6]Department of Molecular Medicine, School of Medicine, University of Utah, Salt Lake City, Utah, USA.

Familial exudative vitreoretinopathy (FEVR) is a severe retinal vascular disease that causes blindness. FEVR has been linked to mutations in several genes associated with inactivation of the Norrin/β-catenin signaling pathway, but these account for only approximately 50% of cases. We report that mutations in α-catenin (*CTNNA1*) cause FEVR by overactivating the β-catenin pathway and disrupting cell adherens junctions. We identified 3 heterozygous mutations in *CTNNA1* (p.F72S, p.R376Cfs*27, and p.P893L) by exome sequencing and further demonstrated that FEVR-associated mutations led to overactivation of Norrin/β-catenin signaling as a result of impaired protein interactions within the cadherin-catenin complex. The clinical features of FEVR were reproduced in mice lacking *Ctnna1* in vascular endothelial cells (ECs) or with overactivated β-catenin signaling by an EC-specific gain-of-function allele of *Ctnnb1*. In isolated mouse lung ECs, both CTNNA1-P893L and F72S mutants failed to rescue either the disrupted F-actin arrangement or the VE-cadherin and CTNNB1 distribution. Moreover, we discovered that compound heterozygous *Ctnna1* F72S and a deletion allele could cause a similar phenotype. Furthermore, in a FEVR family, we identified a mutation of *LRP5*, which activates Norrin/β-catenin signaling, and the corresponding knockin mice exhibited a partial FEVR-like phenotype. Our study demonstrates that the precise regulation of β-catenin activation is critical for retinal vascular development and provides new insights into the pathogenesis of FEVR.

Introduction

Familial exudative vitreoretinopathy (FEVR) is a severe inherited retinal disorder characterized by incomplete vascularization of the peripheral retina and by the absence or abnormality of the secondary and tertiary capillary layers in the deep retina (1). These pathological changes are believed to result in neovascularization and exudate, vitreous hemorrhaging, traction from the vitreous membranes, displacement (ectopia) of the macula, and folding and detachment of the retina (2). FEVR is genetically heterogeneous, and its clinical features can be highly variable; family members with the same mutation can present without symptoms or exhibit a range of clinical features, including complete blindness (3).

FEVR can be inherited as an autosomal-dominant, autosomal-recessive, or X-linked disorder. Mutations in 11 genes and 1 locus have been identified as causing FEVR: low-density lipoprotein receptor–related protein 5 (*LRP5*) (4, 5); frizzled 4 (*FZD4*) (3); Norrin, previously known as Norrie disease pseudoglioma (*NDP*) (6); tetraspanin-12 (*TSPAN12*) (7–9); zinc finger protein 408 (*ZNF408*) (2); kinesin family member 11 (*KIF11*) (10); catenin β 1 (*CTNNB1*) (11, 12); atonal homolog 7 (*ATOH7*) (13); RCC1 and BTB domain–containing protein 1 (*RCBTB1*) (14); exudative vitreoretinopathy 3 (*EVR3*) on chromosome 11p12-13 (15); integrin-linked kinase (*ILK*) (16); and jagged canonical Notch ligand 1 (*JAG1*) (17). In addition to FEVR, *LRP5* mutations are associated with osteopenia and osteoporosis (18), whereas mutations in *NDP* cause Norrie disease, which features intellectual disability (ID) and cognitive impairments (19). Mutations in *KIF11* are also associated with microcephaly, with or without chorioretinopathy, lymphedema, or ID (20), and mutations in *CTNNB1* are associated with syndromic ID (21). Thus, FEVR can feature in syndromes that cause intellectual impairment or disability.

Previous studies have indicated that the pathogenesis of FEVR may involve disrupted Norrin/β-catenin pathway signaling (7, 22–25). Normally, FZD4 and LRP5 form a complex with TSPAN12 in the plasma membrane of endothelial cells (ECs) (7, 22–25). Norrin is an extracellular ligand that binds to FZD4 on ECs with the aid of LRP5 and TSPAN12 to activate downstream β-catenin/Wnt pathway signaling (7, 22–25). Therefore, mutations

Authorship note: Xianjun Zhu and ZY jointly directed this work. Xianjun Zhu, MY, PZ, and SL contributed equally to this work.
Conflict of interest: The authors have declared that no conflict of interest exists.

Submitted: May 4, 2020; **Accepted:** January 22, 2021; **Published:** March 15, 2021.
Reference information: *J Clin Invest*. 2021;131(6):e139869.
https://doi.org/10.1172/JCI139869.

in any of the genes encoding these 5 proteins (*NDP*, *FZD4*, *LRP5*, *TSPAN12*, and β-catenin) might lead to FEVR by inactivating the Norrin/β-catenin pathway and altering the expression of its downstream target genes (7, 22–25). However, it remains unclear how mutations in the *ZNF408*, *KIFF11*, *ATOH7*, and *RCBTB1* genes and *EVR3* on chromosome 11p12-13 contribute to the pathogenesis of FEVR. Mutations in the 11 genes and 1 locus currently associated with FEVR can explain only approximately 50% of FEVR cases (26, 27), so we performed whole-exome sequencing (WES) analysis of 49 FEVR families who do not carry mutations in these genes. From this sequence analysis, we identified 3 heterozygous mutations in α-catenin (*CTNNA1*) of the cadherin-catenin complex associated with the phenotypes of FEVR. CTNNA1 is a core member of the cadherin-catenin complex, which integrates adherens junctions (AJs) with the actin cytoskeleton and promotes intercellular adhesion (28, 29). *CTNNA1* has been reported as a putative tumor suppressor in myeloid leukemia (30), glioblastoma (31), skin cancer (32), and gastric cancer (33, 34). Saskens et al. identified mutations in *CTNNA1* that cause butterfly-shaped pigment dystrophy (35). Very recently, a missense *CTNNA1* mutation was identified in a patient with age-related macular degeneration (AMD) (36). Furthermore, Alexander et al. identified 4 mutations in *CTNNA1* that cause macular pattern dystrophy (37). These findings together introduced a new perspective that *CTNNA1* might affect retinal development. Using a range of approaches, including cell biological assays and genetically modified mouse models, we demonstrate here that the mutant forms of *CTNNA1* identified in our WES analysis disrupt conformation of the cadherin-catenin complex and induce inappropriate overactivation of the Norrin/β-catenin pathway in vascular ECs that causes FEVR.

Results

WES of FEVR families identified mutations in CTNNA1. We performed WES to identify potentially novel genetic mutations in 49 families (14 unaffected individuals and 86 individuals affected with FEVR) with an autosomal-dominant form of FEVR without mutations in known FEVR genes. Variants identified by WES with a frequency of less than 0.005 in the dbSNP138, Exome Variant Server, Exome Aggregation Consortium (ExAC), and Genome Aggregation Database (gnomAD) databases and absent in 1000 sequenced controls were filtered. These filtered variants were then annotated with ANNOVAR software (see Methods for detailed information and see Supplemental Table 1; supplemental material available online with this article; https://doi.org/10.1172/JCI139869DS1). We selected genes that met all 3 of the following standards as the top candidate genes for FEVR (38). First, candidate genes harbored at least 1 "disruptive" variant (nonsense, frameshift, or in splice sites; ref. 39). Second, the variant was present in at least 3 FEVR families. Third, the candidate gene was related to Wnt signaling pathways or angiogenesis. α-Catenin (*CTNNA1*) (3 families) was the best candidate gene in terms of meeting our stringent criteria. From this analysis, 3 heterozygous mutations in *CTNNA1*, a core component of the cadherin-catenin complex, were discovered in 3 families with FEVR: family 3016, family 3004, and family 34 (Figure 1 and Supplemental Tables 2 and 3).

For family 3016 and family 3004, we sequenced both of the affected family members using WES. After filtering coding variants with a minor allele frequency (MAF) above 0.005 in public databases and an in-house database, we ultimately obtained 51 rare variants in family 3016 and 40 rare variants in family 3004, in which the combined annotation–dependent depletion (CADD) scores of 9 and 1 genes were higher than those for *CTNNA1*, respectively. However, *CTNNA1* was the only gene that met the candidate gene selection standard (Supplemental Table 1). For Family 34, we sequenced the proband using WES and found 78 rare variants after filtering coding variants with a MAF of greater than 0.005 in public databases and an in-house database. *CTNNA1* p.R376Cfs*27 is a frameshift mutation that truncates the majority of the CTNNA1 protein domains and most likely disrupts protein function (Supplemental Table 1). Supplemental Table 1 lists all the rare variants in the 3 families. Finally, Sanger sequencing analysis confirmed 3 heterozygous mutations in exon 3 (c.215T>C; p.F72S), exon 8 (c.1125_1131delCAGGGAC; p.R376Cfs*27), and exon 18 (c.2678C>T; p.P893L) of *CTNNA1* in patients with FEVR, but not in the unaffected members of families 3016, 34, and 3004 (Figure 1A). These mutations affect amino acids that are highly conserved in the genes across different species (Figure 1A). The affected parents of the probands lacked peripheral vessels with neovascularization and leakage according to fundus fluorescein angiography (Figure 1C), however, we observed no visible macular abnormality in the fundus examination of these patients (Figure 1D). Notably, we found that the p.R376Cfs*27 mutation led to the most severe phenotype due to complete loss of the CTNNA1 protein (Figure 1C and Supplemental Table 2). However, there we observed no noteworthy clinical phenotype discrepancies between the P893L and F72S mutations.

Mutant CTNNA1 causes overactivation of the β-catenin pathway. α-Catenin (*CTNNA1*) binds to β-catenin (*CTNNB1*) adjacent to the membrane in AJs and to the actin cytoskeleton in the cytoplasm, whereas β-catenin (*CTNNB1*) binds to the cytoplasmic domain of VE-cadherin (*CDH5*) to form a cadherin-catenin complex (40, 41). α-Catenin and VE-cadherin also regulate Wnt signaling through their interactions with β-catenin by segregating the available pool of β-catenin in the cytosol, thereby inhibiting the expression of downstream genes (42–45). To assess the effect of the *CTNNA1* mutations on the biological functions of α-catenin, we used site-directed mutagenesis to introduce the 3 mutations identified in the FEVR families into *CTNNA1* expression plasmids. First, we asked whether the mutant α-catenin proteins interacted normally with β-catenin. The coimmunoprecipitation results showed that the F72S mutant form of α-catenin completely failed to interact with β-catenin, whereas the P893L mutant retained the interaction (Figure 2A). The frameshift mutation (p.R376Cfs*27) of *CTNNA1* resulted in nonsense-mediated decay, because no protein could be identified by Western blot (Figure 2A). Therefore, 2 of the 3 α-catenin mutant proteins diminished their normal interactions with β-catenin. Next, we investigated the potential effects of the identified mutant α-catenin protein on the Norrin/β-catenin pathway. To this end, we compared Norrin/FZD4/LRP5/β-catenin signaling in the presence or absence of the WT and mutant forms of *CTNNA1* using the TopFlash reporter gene system, in which luciferase levels represent signaling pathway activity. Expression of the WT *CTNNA1* in human embryonic kidney 293 (HEK293) SuperTopFlash (STF) cells led to diminished luciferase activi-

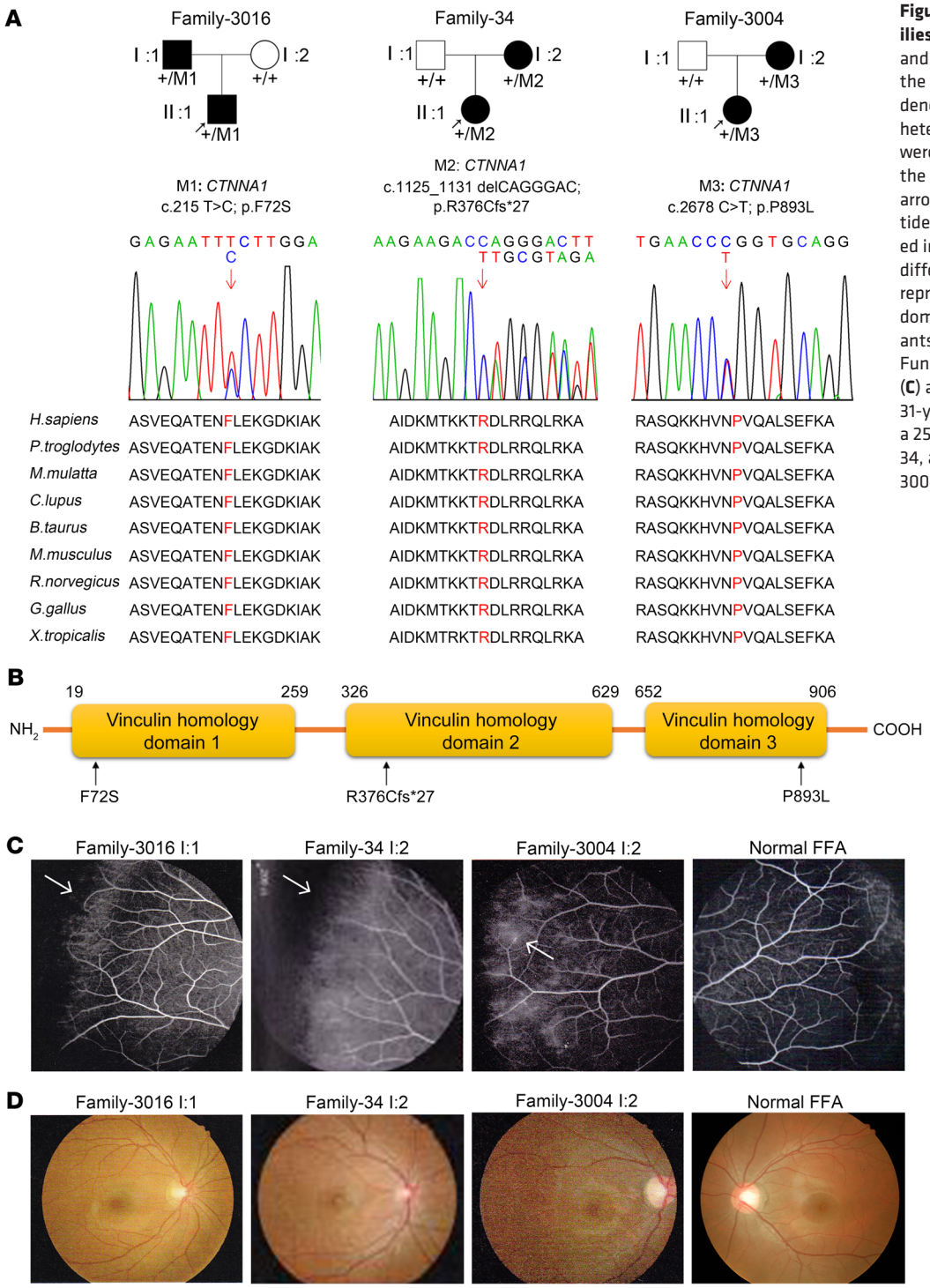

Figure 1. *CTNNA1* mutations in families with FEVR. (**A**) FEVR pedigrees and Sanger sequencing analysis show the inheritance of FEVR (patients are denoted with black symbols). Three heterozygous mutations in *CTNNA1* were identified. Black arrows indicate the proband of each family. Red arrows indicate the changed nucleotides. Affected amino acids are denoted in red and are conserved among different species. (**B**) Schematic representation of the CTNNA1 protein domains showing the location of variants identified in this study. (**C** and **D**) Fundus fluorescein angiography (FFA) (**C**) and fundus photography (**D**) of a 31-year-old patient (I:1) in family 3016, a 25-year-old patient (I:2) in family 34, a 27-year-old patient (I:2) in family 3004, and a normal individual.

ty compared with that in cells transfected with an empty vector (Figure 2B), confirming the inhibitory role of α-catenin in Norrin/β-catenin transcriptional activity (42–45). However, Norrin/β-catenin signaling pathway activity was significantly increased upon expression of each of the mutant α-catenin proteins (Figure 2B). Compared with their WT protein, the P893L mutant of *CTNNA1* showed an approximately 1.3-fold increase in Norrin/β-catenin transcriptional activity. Both F72S and the R376Cfs*27 mutation of *CTNNA1* completely failed to inhibit Norrin/β-catenin transcriptional activity, suggesting that the mutant α-catenin proteins might fail to control the available pool of β-catenin in the cytosol.

To explore whether *CTNNA1* mutants could affect endogenous β-catenin transcriptional activity, we performed adenovirus-directed overexpression of WT or mutant *CTNNA1* in human retinal endothelial cells (HRECs). Quantitative real-time PCR (qPCR) analysis was applied to detect changes in mRNA levels of β-catenin downstream genes, including cyclin D1 (*CCND1*), c-Myc (*MYC*), occludin (*OCLN*), and claudin 5 (*CLDN5*). As shown in

Supplemental Figure 1, overexpression of WT *CTNNA1* significantly reduced the transcript levels of these genes compared with that transfected with vector plasmids. Mutant forms of *CTNNA1* significantly increased the transcript levels of these genes compared with WT *CTNNA1*, consistent with the notion that CTNNA1 inhibits β-catenin activity (Figure 2B).

To confirm the involvement of α-catenin in Norrin/β-catenin pathway regulation, we assayed β-catenin activity using the TopFlash reporter gene system following lentivirus-mediated shRNA knockdown (KD) of *CTNNA1* in HEK293 STF cells. The KD efficacy of *CTNNA1* in HEK293 STF cells was 87% (Figure 2C). We observed a 6-fold increase in Norrin/β-catenin transcriptional activity in *CTNNA1*-silenced cells compared with the activity measured in cells treated with a control shRNA (Figure 2D). Moreover, mRNA levels of endogenous β-catenin–regulated genes (*CCND1*, *MYC*, *OCLN*, and *CLDN5*) in *CTNNA1*-KD or *CTNNB1* overexpressed HRECs were detected using qPCR. We detected a significant elevation of mRNA levels of these genes in both *CTNNA1*-KD and *CTNNB1*-overexpressed HRECs compared with control mRNA levels (Supplemental Figure 2). Consistent with previous findings (43–45), these results provide support for the role of *CTNNA1* in inhibiting Norrin/β-catenin signaling. Hence, the dysfunction of *CTNNA1* resulted in overactivation of the Norrin/β-catenin pathway.

Dysfunction of CTNNA1 interrupts cell AJs. We next transfected adenoviruses containing mutant *CTNNA1*-F72S and *CTNNA1*-R893L into HRECs to test whether this mutant allele interferes with normal cell assembly and the stability of AJs in these retinal ECs. When transiently overexpressed in HRECs, the *CTNNA1*-P893L mutant and WT proteins were correctly localized in the plasma membrane, whereas the *CTNNA1*-F72S mutant protein was localized in the cytosol of HRECs. Expression of both *CTNNA1*-P893L and *CTNNA1*-F72S led to disruption of F-actin filament organization compared with the WT CTNNA1 protein (Figure 2E). To assess the effect of *CTNNA1* deficiency on AJs, we used the lentivirus-mediated shRNA to knock down *CTNNA1* in HRECs. As shown in Figure 3, A and B, *CTNNA1* expression in KD cells was reduced to approximately 10% of that observed in control cells. Under normal culture conditions, VE-cadherin between ECs forms a confluent junction at the cell membrane but is prominently reduced after *CTNNA1* KD (Figure 3C). δ-Catenin (also known as p120-catenin or CTNND1; referred to hereafter as CTNND1), a protein that binds to and suppresses VE-cadherin endocytosis, was also discontinuous and reduced on the plasma membrane following *CTNNA1* KD (Figure 3D and ref. 46). Moreover, we found that membrane expression of β-catenin was also reduced in *CTNNA1*-KD cells (Figure 3E). This indicates that normal CTNNA1 levels on the cell membrane are important for maintaining the stability of AJ proteins at cell junctions. In addition, we observed severe disorganization of F-actin in the *CTNNA1*-KD cells compared with control cells, further supporting the hypothesis that dysfunction of CTNNA1 impairs both AJs and the actin cytoskeleton. Furthermore, we found that KD of *CDH5* or *CTNND1* in HRECs resulted in phenotypes similar to those seen in *CTNNA1*-KD cells, suggesting the essential role of core components in the cadherin-catenin complex (Figure 3).

Because disruption of the cadherin-catenin complex might release β-catenin from the cell membrane and activate Wnt signaling, which regulates cell proliferation (43–45), we sought to determine whether KD of *CTNNA1* in HRECs could promote proliferation using a 5-ethynyl-2′-deoxyuridine (EdU) incorporation assay. As expected, we found increased proliferation upon *CTNNA1* KD (Supplemental Figure 3), which is consistent with studies demonstrating that CTNNA1 acts as a tumor suppressor and that depletion of *CTNNA1* leads to increased cell proliferation in vitro (32, 34).

Loss of Ctnna1 in vascular ECs causes angiogenesis defects in mouse retinas. We then investigated whether loss of *Ctnna1* in mouse vascular ECs could lead to FEVR phenotypes using genetically modified mouse models. *Ctnna1* is essential for early development, and its deletion in vascular ECs using conditional *Ctnna1*-KO mice and *Tie2-Cre*–transgenic mice resulted in embryonic lethality (Supplemental Table 4). To overcome this problem, we generated an inducible endothelial KO mouse model by crossing mice carrying the *Ctnna1* floxed allele with mice carrying *Pdgfb-iCreER*, in which Cre is fused to ERT2 and expressed under the control of the *Pdgfb* promoter. $Ctnna1^{fl/fl}$, *Pdgfb-iCre-ER*, and $Ctnna1^{fl/fl}$ or *Pdgfb-iCre-ER* littermate controls were given daily i.p. injections of tamoxifen for 4 days, starting on P1. The specificity of Cre-mediated recombination was evaluated using the tdTomato reporter (Supplemental Figure 4A). After induction by tamoxifen, *Ctnna1* was deleted in the ECs of $Ctnna1^{fl/fl}$ *Pdgfb-iCre-ER* mice (hereafter termed $Ctnna1^{iECKO/iECKO}$), with the expression of tdTomato restricted to ECs (Supplemental Figure 4A). Tamoxifen-treated $Ctnna1^{fl/fl}$ or *Pdgfb-iCre-ER* mice were used as WT controls.

Following the administration of tamoxifen from P1 to P4, the $Ctnna1^{iECKO/iECKO}$ mice were smaller in body size, with a decrease in body weight of approximately 22% (Supplemental Figure 4, B and C), and failed to thrive. Most of them died by P9 (Supplemental Table 5), indicating the blunted overall body development upon complete depletion of *Ctnna1* in murine ECs. The external appearance of the heterozygous $Ctnna1^{iECKO/+}$ mice was similar to that of their WT littermates (Supplemental Figure 4B). Areas of bleeding were apparent in the eyeballs of $Ctnna1^{iECKO/iECKO}$ mice (Supplemental Figure 4D), a phenomenon also observed in patients with FEVR (Figure 1C), indicating that *Ctnna1* plays a role in retinal vascular development. In addition, the eyeballs of $Ctnna1^{iECKO/iECKO}$ mice were smaller than those of their littermate controls, indicating that the development of the retinal vasculature may affect eye size (Supplemental Figure 4, D and E). Bright-field imaging of the retinas and hyaloid vessels of *Ctnna1*-mutant mice revealed abnormal, blood-red vessel structures (Supplemental Figure 4D). The hyaloid vasculature of $Ctnna1^{iECKO/iECKO}$ mice had a phenotype similar to that of $Norrin^{-/-}$ (47), $Lrp5^{-/-}$ (48), $Tspan12^{-/-}$ (7), and $Fzd4^{-/-}$ (24) mice, characterized by its slower regression by P9 compared with littermate controls (Figure 4A). These data suggested that the loss of *Ctnna1* might disrupt normal apoptosis-mediated regression of hyaloid vessels.

Flat-mounted retinas obtained from $Ctnna1^{iECKO/iECKO}$ and control mice were evaluated using isolectin B4 (IB4), which labels blood vessel cells. At P3, the horizontal growth of blood vessels was slower in $Ctnna1^{iECKO/iECKO}$ mice than that in WT controls (Supplemental Figure 4, F and G). At P9, the superficial vessels of $Ctnna1^{iECKO/iECKO}$ mice were markedly enlarged during development, accompanied by delayed horizontal outgrowth and hyperplasia (Figure 4, B–D, G, and H, and Supplemental Figure 4H).

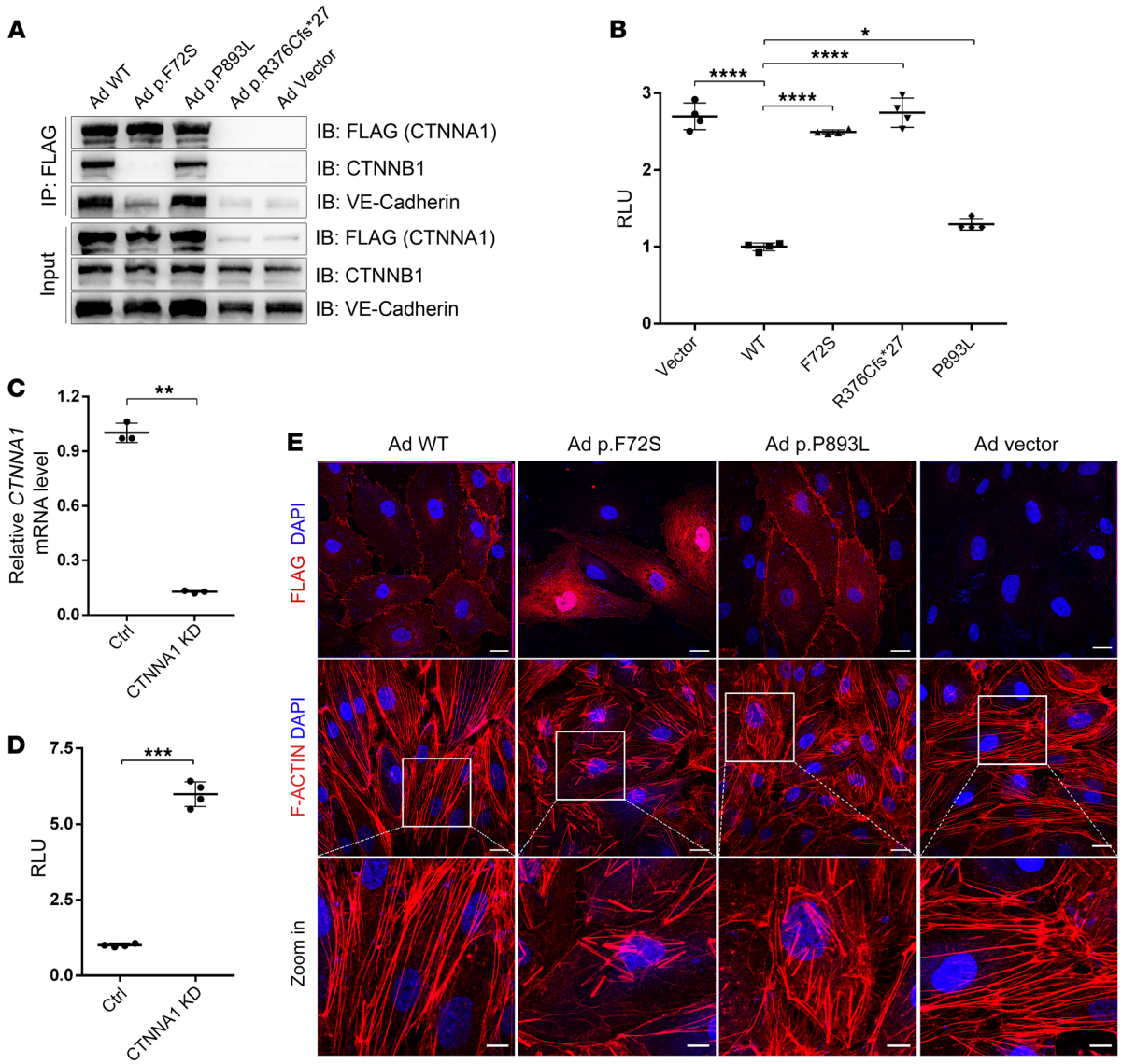

Figure 2. *CTNNA1* mutations result in Norrin/β-catenin signaling overactivation, α-catenin mislocalization, and F-actin disorganization. (**A**) Western blot analysis of CTNNA1 (WT and mutants) coimmunoprecipitated with CTNNB1 and VE-cadherin. An empty vector was used as a negative control. (**B**) Results of a luciferase reporter assay in HEK293 STF cells. Cells were transfected with plasmids containing *CTNNA1* (WT, p.F72S, p.R376C*fs27, or p.P893L) or an empty vector (pCDNA3.1). Plasmids were cotransfected with *LRP5*, *FZD4*, *NDP*, and *Renillareniformis* (PGL4.1). The activity of WT protein was normalized to 1. Error bars indicate the SD. $^{*}P < 0.05$ and $^{****}P < 0.0001$, by 1-way ANOVA with Dunnett's multiple-comparison test ($n = 4$). (**C**) qPCR analysis demonstrated efficient shRNA-mediated KD of *CTNNA1* in HEK293 STF cells. Error bars indicate the SD. $^{**}P < 0.01$, by Student's *t* test ($n = 3$). (**D**) ShRNA-mediated KD of *CTNNA1* in the HEK293 STF cell line led to elevated luciferase activity. Error bars indicate the SD. $^{***}P < 0.001$, by Student's *t* test ($n = 4$). (**E**) Adenovirus-mediated (Ad-mediated) overexpression of WT and mutant CTNNA1 (F72S, P893L) in HRECs. Costaining with DAPI and anti-Flag (CTNNA1) or F-actin antibody was performed. Scale bars: 25 μm and 10 μm (enlarged insets). Experiments were performed independently at least 3 times.

Interestingly, unlike *Fzd4*$^{+/-}$ (24), *Lrp5*$^{+/-}$ (47), and *Tspan12*$^{+/-}$ (7) mice, the vasculature of heterozygous *Ctnna1*$^{iECKO/+}$ retinas also showed moderately delayed radial outgrowth, indicating that angiogenesis is more sensitive to *Ctnna1* dosage than to the dosages of the above-mentioned genes (Figure 4, B and G). This is consistent with the fact that heterozygous *CTNNA1* mutations causes FEVR in humans. To further characterize the above-mentioned phenotypes, we performed an immunofluorescence staining assay on frozen retinal sections. In control mice, we found that vertical branches formed from the primary vasculature at P9 and subsequently established capillaries in the outer and inner plexiform layers (OPL and IPL) (Figure 4C and Supplemental Figure 4H, left panels). However, the loss of 1 copy of *Ctnna1* delayed vertical growth of the superficial retina vascular plexus (Figure 4C and Supplemental Figure 4H, middle panels). Both *Ctnna1*$^{iECKO/iECKO}$ and *Ctnna1*$^{iECKO/+}$ retinas had obvious defects in vertical vascular growth into the deeper retinal layers and hyperplasia of the vascular plexus, and both also lacked vertical secondary and tertiary vessels at P9 (Figures 4C and Supplemental Figure 4H, right panels).

Given that adult *Fzd4*$^{-/-}$, *Ndp*$^{-}$, and *Tspan12*$^{-/-}$ retinas completely lack deep vessel layers (7, 25), we asked whether adult mice have a similar phenotype upon homozygous or heterozy-

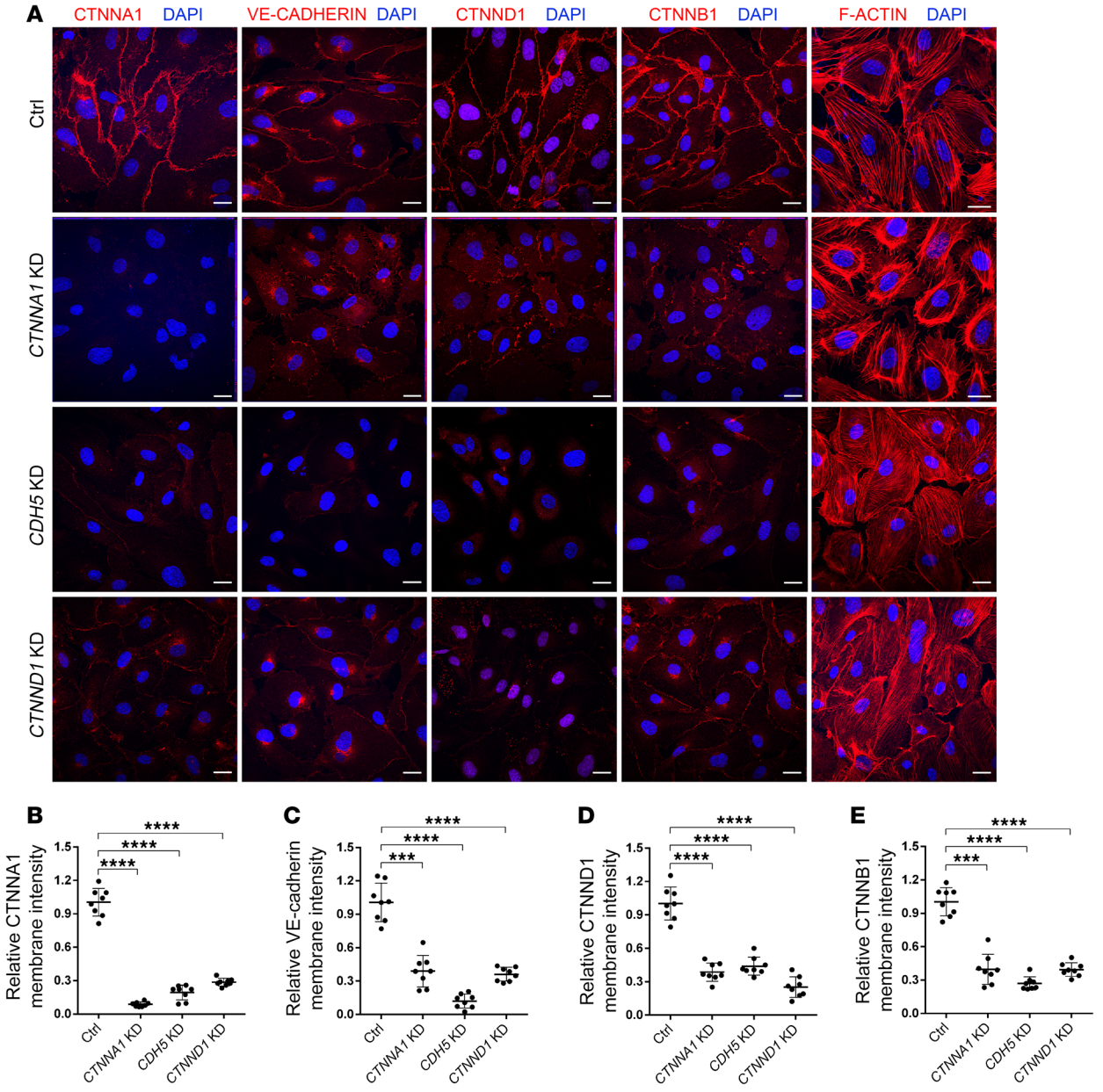

Figure 3. CTNNA1, CDH5, and CTNND1 are essential for the integrity of the cadherin-catenin complex in HRECs. (**A**) Immunofluorescence images of HRECs transfected with an shRNA targeting *CTNNA1*, *CDH5*, and *CTNND1* or a control shRNA. Anti-CTNNA1, VE-cadherin, CTNND1, CTNNB1, or F-actin antibody (red) was costained with DAPI (blue). Scale bars: 25 μm. (**B**–**E**) Quantification of membrane signal intensity of CTNNA1, VE-cadherin, CTNND1, and CTNNB1 in *CTNNA1*-, *CDH5*-, *CTNND1*-KD, and control (Ctrl) HRECs. Error bars indicate the SD. ***$P < 0.001$ and ****$P < 0.0001$, by 1-way ANOVA with Dunnett's multiple-comparison test ($n = 8$). Experiments were performed independently at least 3 times.

gous depletion of *Ctnna1* in ECs. Because *Ctnna1*$^{iECKO/iECKO}$ mice died at approximately P9 when tamoxifen was injected starting on P1, we gave tamoxifen injections beginning on P6 and found that *Ctnna1*$^{iECKO/iECKO}$ mice died between P13 and P14 (Supplemental Table 6). It was previously reported that the retinal vasculature of mice develops through 3 stages: superficial radial growth from P1 to P9, development of the deep vessel plexus in the OPL from P7 to P12, and growth of the intermediate vessel plexus in the IPL from P11 to P17 (49). Thus, we chose P13 as a checkpoint for deep vessel development. Interestingly, *Ctnna1*$^{iECKO/iECKO}$ mice (tamoxifen induction from P6) showed abnormalities only at the periphery of the superficial vasculature at P13 (Supplemental Figure 5), suggesting that CTNNA1 might mostly affect tip cell vessel development rather than stalk cell vessel stability. Notably, at P13 we found fewer vessels in the OPL and minimal vessels in the IPL of *Ctnna1*$^{iECKO/iECKO}$ retinas compared with that observed in control retinas (Supplemental Figure 5, B and C). However, at P13, *Ctnna1*$^{iECKO/+}$ mice showed only mild delay in vessel development in the IPL of the retina compared with control retinas (Supplemental Figure 6). Therefore, loss of *Ctnna1* in mouse retinal vascular cells led to angiogenesis defects and partially reproduced clinical features seen in FEVR patients.

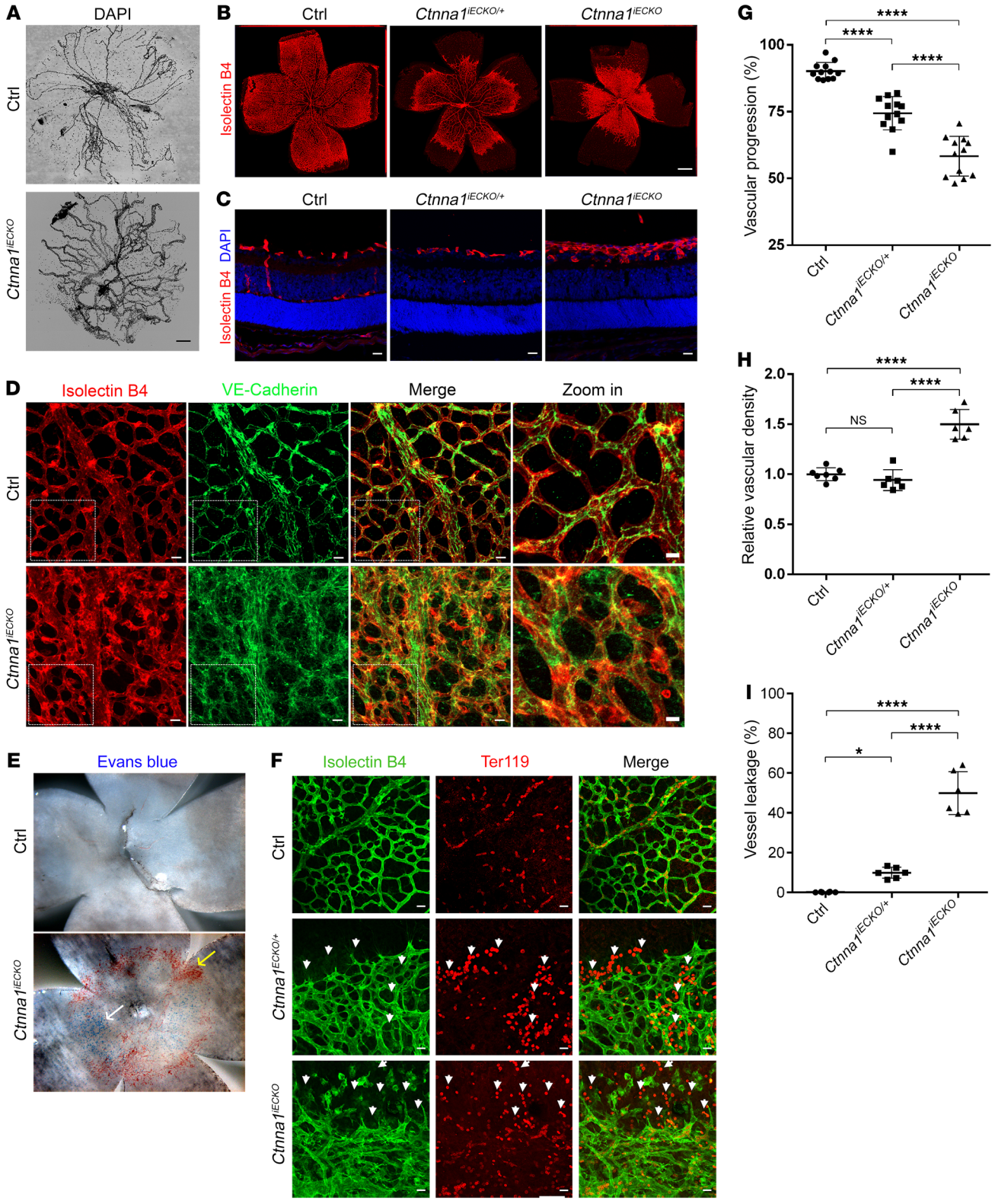
A
DAPI
Ctrl
Ctnna1iECKO
B
Ctrl
Ctnna1iECKO/+
Ctnna1iECKO
Isolectin B4
C
Ctrl
Ctnna1iECKO/+
Ctnna1iECKO
Isolectin B4 DAPI
D
Isolectin B4
VE-Cadherin
Merge
Zoom in
Ctrl
Ctnna1iECKO
E
Evans blue
Ctrl
Ctnna1iECKO
F
Isolectin B4
Ter119
Merge
Ctrl
Ctnna1iECKO/+
Ctnna1iECKO
G
Vascular progression (%)
100
75
50
25
****
****
****
Ctrl
Ctnna1iECKO/+
Ctnna1iECKO
H
Relative vascular density
2.0
1.5
1.0
0.5
0.0
****
****
NS
Ctrl
Ctnna1iECKO/+
Ctnna1iECKO
I
Vessel leakage (%)
100
80
60
40
20
0
****
****
*
Ctrl
Ctnna1iECKO/+
Ctnna1iECKO

Figure 4. Conditional KO of *Ctnna1* in mice causes severe retinal vascularization defects. (**A**) DAPI staining of hyaloid vessels in the eyes of control and *Ctnna1*^{iECKO} mice, showing that hyaloid vessel regression was markedly delayed in the eye. Scale bar: 250 μm. (**B**) Compared with those of littermate controls, P9 flat-mounted retinas of *Ctnna1*$^{iECKO/+}$ mice showed delayed radial growth of the superficial vascular plexus, with moderate neovascularizations at the angiogenic front. *Ctnna1*^{iECKO} retinas showed retarded vascular growth and hyperplasia of the primary vascular plexus. Vessels were stained with IB4 (red). Scale bar: 500 μm. (**C**) Frozen sections of retinas from P9 control, *Ctnna1*$^{iECKO/+}$, and *Ctnna1*^{iECKO} mice were costained with IB4 (red) and DAPI (blue). Scale bars: 25 μm. Vertical growth of the superficial retinal vascular plexus was delayed in *Ctnna1*$^{iECKO/+}$ mice. In *Ctnna1*^{iECKO} retinas, profound defects in vertical vascular growth into the deeper retinal layers were observed, and the vascular plexus became hyperplastic. No secondary or tertiary vessels were observed in these retinas. (**D**) VE-cadherin (green) and IB4 (red) staining of P9 *Ctnna1*^{iECKO} and control retinas. VE-cadherin was disorganized in *Ctnna1*^{iECKO} retinas. White dotted boxes indicate enlarged regions, detailed on the right. Scale bars: 25 μm and 10 μm (enlarged insets). (**E**) P9 flat-mounted *Ctnna1*^{iECKO} retinas showed extensive leakage of Evans blue dye (white arrow) and visible, enlarged blood vessels (yellow arrow) compared with control retinas. (**F**) *Ctnna1*^{iECKO}, *Ctnna1*$^{iECKO/+}$, and control retinas were costained with IB4 (green) and Ter119 (red), revealing extensive leakage of erythrocytes (white arrowheads) in *Ctnna1*$^{iECKO/+}$ and *Ctnna1*^{iECKO} retinas. Scale bars: 25 μm. (**G**–**I**) Quantification of vascular progression, vascular density, and vessel leakage. Error bars indicate the SD. $^{*}P < 0.05$ and $^{****}P < 0.0001$, by 1-way ANOVA with Tukey's multiple-comparison test ($n \geq 6$). Experiments were performed independently at least 3 times.

In addition, VE-cadherin also appeared diffuse in *Ctnna1*$^{iECKO/iECKO}$ mice retinas (Figure 4D), further supporting a role of CTNNA1 in the stability of catenin/cadherin complex and normal retinal angiogenesis. In *Ctnna1*$^{iECKO/iECKO}$ retinas, staining with small-molecule Evans blue dye (MW = 961 g/mol) and of red blood cells with a Ter119 antibody revealed a 50% increase in leakage along blood vessels (Figure 4, E, F, and I), providing evidence of exudative bleeding from retinal vessels. Electron microscope ultrastructural analysis also revealed discontinuous distribution of EC-EC tight junctions (Supplemental Figure 7). In addition, we observed glial fibrillary acidic protein (GFAP) accumulation in *Ctnna1*$^{iECKO/iECKO}$ retinas (Supplemental Figure 8A), resembling the phenotype of *Fz4*$^{-/-}$ mice (24). This accumulation was indicative of activated glial cells and high retinal stress (24). We also detected the tip cell marker Esm1 in the remodeling plexus of *Ctnna1*$^{iECKO/iECKO}$ retinas (Supplemental Figure 8B), indicating an abundance of tip over stalk cells in the plexus (50). Expression of the tight junction protein claudin 5, which is also a Wnt downstream target, was increased with an abnormal distribution pattern in *Ctnna1*$^{iECKO/iECKO}$ retinas (Supplemental Figure 8C). Therefore, loss of *Ctnna1* led to leakage in retinal vessels, similar to the symptoms observed in patients with FEVR.

Loss of Ctnna1 leads to overproliferation of retinal vessels in mouse retinas. To further investigate the consequences of loss of *Ctnna1* in retinal vascular vessels, we analyzed the mitotic proliferation of vascular ECs using an EdU incorporation assay in WT control versus *Ctnna1*$^{iECKO/iECKO}$ and *Ctnna1*$^{iECKO/+}$ retinas at P5 (Figure 5). In P5 *Ctnna1*$^{iECKO/iECKO}$ retinas, we found that EdU-labeled EC proliferation was significantly increased compared with ECs in WT control and *Ctnna1*$^{iECKO/+}$ retinas (Figure 5, A and B), which was similar to the observed overproliferation in *CTNNA1*-KD HRECs (Supplemental Figure 3). These results indicated that uncontrolled proliferation might contribute to vascular remodeling and vessel hyperplasia. We further compared the retinal vascularization of P5 *Ctnna1*$^{iECKO/iECKO}$ mice with that of *Lrp5*- or *Fzd4*-KO mice (a model of FEVR with inactivation of β-catenin signaling) and observed very similar phenotypes, such as delayed superficial vascular progression, neovascularization at the peripheral region, and extensive erythrocyte leakage (Figure 6). However, compared with WT control retinas, the vessel density of *Ctnna1*$^{iECKO/iECKO}$ retinas was evidently increased, whereas it was decreased in *Lrp5*- and *Fzd4*-KO retinas (Figure 6C). EC proliferation is induced by vascular endothelial growth factor A (VEGFA) (51. We measured the abundance of VEGFA (VEGF164) in *Ctnna1*$^{iECKO/iECKO}$ and control retinas. In the control retinas, VEGFA was expressed ahead of the angiogenic front (Figure 7A, left panel), and a very low abundance of VEGFA was detected in the remodeling plexus. However, in *Ctnna1*$^{iECKO/iECKO}$ retinas, we detected abnormal expression of VEGFA around the angiogenic front and in the remodeling plexus (Figure 7A, right panel). These data indicated that VEGFA was induced by the remodeling plexus after *Ctnna1* deletion. In contrast, we found no difference in VEGFA abundance around the angiogenic front or in the remodeling plexus in *Lrp5*- and *Fzd4*-KO retinas (Figure 7, B and C). During sprouting angiogenesis, the behaviors of tip cells at the front and trailing stalk cells are controlled by VEGFR2 and Notch signaling (52). We detected upregulation of DLL4 in *Ctnna1*$^{iECKO/iECKO}$ retinas (Supplemental Figure 9). In contrast, DLL4 expression was diminished in the vasculature of *Lrp5*- and *Fzd4*-KO retinas (Supplemental Figure 9). These data suggested that the molecular events underlying angiogenesis defects in *Ctnna1*$^{iECKO/iECKO}$ and *Lrp5*- or *Fzd4*-KO retinas are distinct.

Loss of Ctnna1 disrupts the integrity of the blood-brain barrier in mice. The integrity of the blood-brain barrier (BBB) is important for central nervous system function. We therefore tested whether loss of *Ctnna1* damages the BBB. Obvious bleeding regions were observed in the brains of *Ctnna1*$^{iECKO/iECKO}$ mice (Supplemental Figure 10A), most prominently in the cerebellum, implying the occurrence of blood vessel leakage in the brain. To determine whether BBB integrity was disrupted during postnatal angiogenesis in *Ctnna1*$^{iECKO/iECKO}$ mice, we injected them i.p. with Evans blue dye on P8, 24 hours before sacrifice. As predicted, we observed extensive leakage of Evans blue throughout the brains of *Ctnna1*$^{iECKO/iECKO}$ mice (Supplemental Figure 10A), indicating a disruption of the entire BBB. We also examined H&E-stained paraffin-embedded sections of *Ctnna1*$^{iECKO/iECKO}$ mouse brains (Supplemental Figure 10B), and found that deletion of *Ctnna1* resulted in an altered morphology of the cerebellum compared with that of littermate controls. We also observed regions of hemorrhage in the *Ctnna1*$^{iECKO/iECKO}$ cerebellum (Supplemental Figure 10B). Next, we imaged the cerebellum in P9 animals using contrast-enhanced x-ray microcomputed tomography (micro-CT) to examine abnormal blood vessels. Sagittal projections of the *Ctnna1*$^{iECKO/iECKO}$ and control cerebellums are shown in Supplemental Figure 10C. Compared with WT controls, the *Ctnna1*$^{iECKO/iECKO}$ cerebellum showed additional high-intensity areas, which were reconstituted in 3D and shown to be widely distributed, abnormal tube-like structures (Supplemental Figures 10D and Supplemental Figure 11A). Because blood-filled lesions were imaged as high-intensity areas, we concluded that

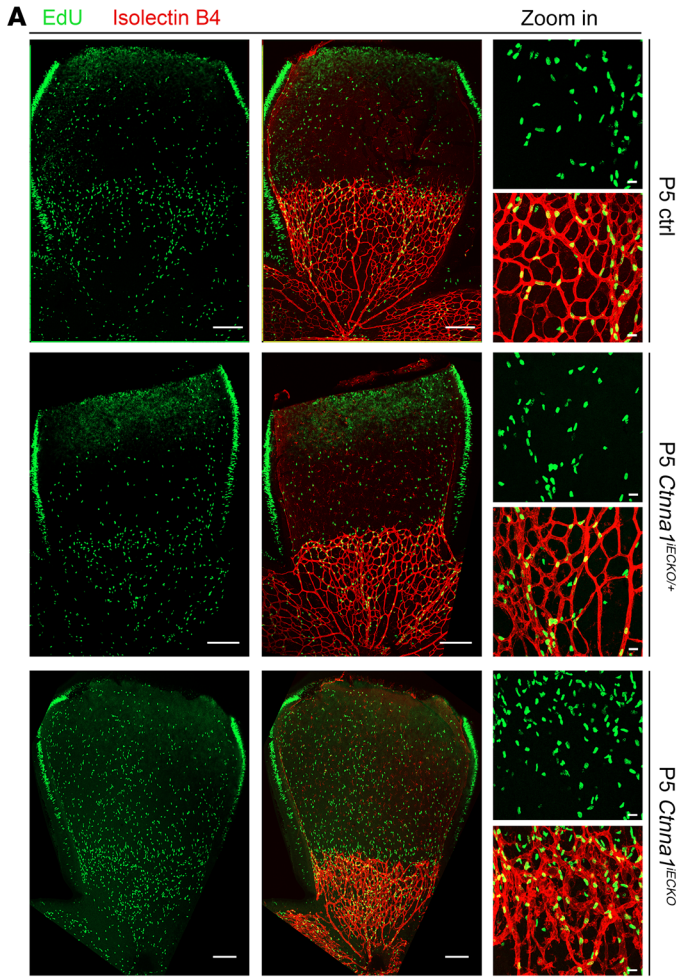

Figure 5. *Ctnna1* deletion in mouse ECs increases their proliferation at P5. (**A**) Vascular cell proliferation of control, *Ctnna1*$^{iECKO/+}$, and *Ctnna1*$^{iECKO/iECKO}$ mice at the vitreal surface was measured with EdU labeling on P5. Images captured at higher magnification are shown in the right panel. Scale bars: 250 μm and 25 μm (enlarged insets). (**B**) Quantification of EdU-positive cells per vascular area. Error bars indicate the SD. ***$P < 0.001$ and ****$P < 0.0001$, by 1-way ANOVA with Tukey's multiple-comparison test ($n = 5$ mice for each group). Experiments were performed independently at least 3 times.

they represented enlarged blood vessels in the *Ctnna1*$^{iECKO/iECKO}$ cerebellum, whereas low-intensity holes are considered edematous lesions (53). The presence of positive Ter119 signals outside of the vessels on frozen sections of the *Ctnna1*$^{iECKO/iECKO}$ cerebellum suggested extensive leakage of erythrocytes from blood vessels (Supplemental Figure 10, E and F, and Supplemental Figure 11B). In addition, we observed enlarged blood vessels and edema-like cavities in these cerebellum sections, consistent with the micro-CT observations of the *Ctnna1*$^{iECKO/iECKO}$ cerebellum (Supplemental Figure 10D). Brain glial cells were also activated, as reflected by the increased levels of GFAP expression in the *Ctnna1*$^{iECKO/iECKO}$ cerebellum (Supplemental Figure 11B). Furthermore, electron microscope ultrastructural analysis confirmed *Ctnna1*$^{iECKO/iECKO}$ cerebellum vessel junctional defects, which included discontinuous distribution of electron-dense tight junctions or leakage of erythrocytes out of vessels (Supplemental Figure 12). Thus, the loss of *Ctnna1* in mice disrupted the integrity of the BBB and impaired the cerebellum's normal structure and functions, similar to the phenotypes observed in the *Fzd4*$^{-/-}$ mice (24).

Loss of Cdh5 in retinal vascular ECs causes angiogenesis defects in mouse retinas. Because KD of *CTNNA1* in ECs reduced the abundance of membrane CDH5 (Figure 3), which is a core component of the cadherin-catenin complex and was previously reported to play an important role in retinal vascular development, we analyzed angiogenesis in detail by breeding mice carrying a *loxP*-flanked *Cdh5* allele with tamoxifen-inducible *Pdgfb-iCre*–transgenic mice to generate *Cdh5*$^{loxp/loxp}$ *Pdgfb-iCreER* (named *Cdh5*$^{iECKO/iECKO}$ mice) (54, 55). We found extensive erythrocyte leakage as well as delayed superficial outgrowth and local hyperdensity of the retinal vasculature in *Cdh5*$^{iECKO/iECKO}$ mice (Supplemental Figure 13A), consistent with the phenotype previously reported and closely resembling the phenotype of *Ctnna1*$^{iECKO/iECKO}$ mouse retinas (54, 55). Furthermore, we observed delayed regression of hyaloid vessels in *Cdh5*$^{iECKO/iECKO}$ mice (Supplemental Figure 13B), suggesting that disruption of the cadherin-catenin complex might cause FEVR.

CDH5 plays an inhibitory role in Norrin/β-catenin signaling. We then asked whether CDH5, like CTNNA1, inhibits Norrin/β-catenin signaling activity. A TopFlash reporter gene assay was applied to demonstrate the effect of CDH5 on Norrin/β-catenin transcriptional activity. Overexpression of *CDH5* in HEK293 STF cells downregulated Norrin/β-catenin signaling activity by approximately 70% compared with that in cells transfected with an empty vector (Supplemental Figure 13C). Moreover, after knocking down *CDH5* (82% reduction in *CDH5* transcriptional levels), we detected a 3.5-fold increase in Norrin/β-catenin transcriptional activity in HEK293 STF cells compared with control cells (Supplemental Figures 13, D and E). These results indicated that *CDH5* plays a role similar to that of *CTNNA1* in regulating Norrin/β-catenin signaling activity.

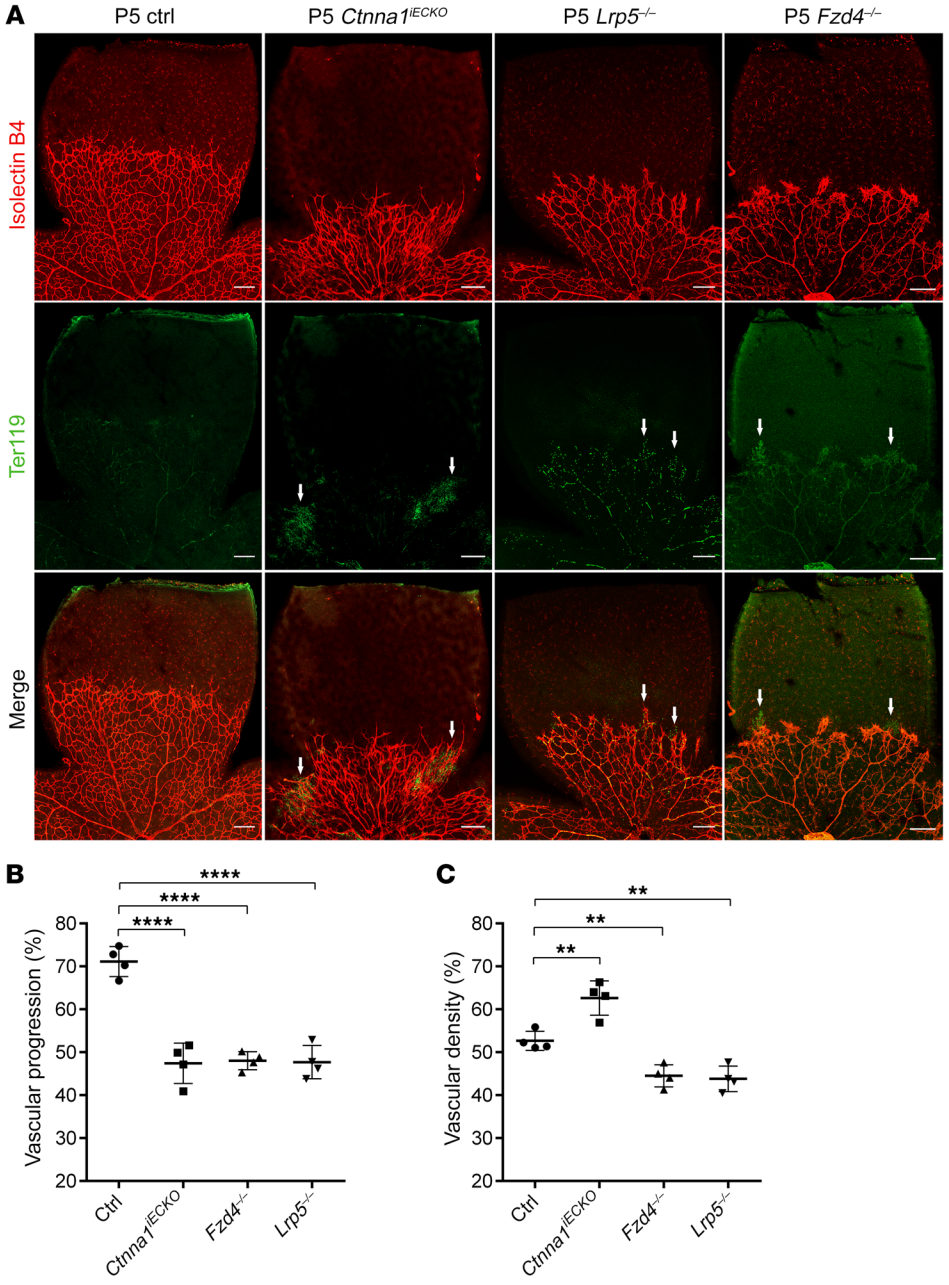

Figure 6. Comparison of retinal vascular phenotypes of *Ctnna1* endothelial conditional KO, *Lrp5*-KO, and *Fzd4*-KO mice. (**A**) P5 *Ctnna1*^{iECKO}, *Lrp5*$^{-/-}$, and *Fzd4*$^{-/-}$ mice had similar phenotypes, such as delayed superficial vascular progression, neovascularization in the peripheral region, and extensive erythrocyte leakage. However, compared with control retinas, the vascular density was increased in *Ctnna1*^{iECKO} retinas but was decreased in *Lrp5*$^{-/-}$ and *Fzd4*$^{-/-}$ retinas. White arrows denote leakage areas. Scale bar: 250 μm. Quantification of vascular progression (**B**) and density (**C**). Error bars indicate the SD. $^{**}P < 0.01$ and $^{****}P < 0.0001$, by 1-way ANOVA with Dunnet's multiple-comparison test ($n = 4$). Experiments were performed independently at least 3 times.

Loss of Ctnna1 or Cdh5 in isolated mouse lung ECs interrupts cell AJs. Because KD of *CTNNA1* or *CDH5* in HRECs disrupted cell AJ proteins (Figure 3), we sought to determine whether the same phenotype could be observed in isolated *Ctnna1*$^{iECKO/iECKO}$ or *Cdh5*$^{iECKO/iECKO}$ mouse lung endothelial cells (MLECs). As Supplemental Figure 14A shows, deletion of endothelial *Ctnna1* resulted in a discontinuous distribution of VE-cadherin, CTNND1, and CTNNB1. Membrane-bound CTNNA1 protein levels were reduced by 89% (Supplemental Figure 14, A and B), indicating efficient *Ctnna1* deletion in MLECs. The levels of membrane-bound VE-cadherin, CTNND1, and CTNNB1 protein in *Ctnna1*$^{iECKO/iECKO}$ MLECs were reduced by 56%, 69%, and 62%, respectively. Similarly, deletion of endothelial *Cdh5* resulted in discontinuous distribution of VE-cadherin, CTNND1, and β-catenin (Supplemental Figure 14, A and C). The membrane-bound protein levels of VE-cadherin were reduced by 81% (Supplemental Figure 14C), also suggesting efficient *Cdh5* excision. Membrane-bound CTNNA1, CTNND1, and CTNNB1 protein levels in *Cdh5*$^{iECKO/iECKO}$ MLECs were reduced by 52%, 64%, and 65%, respectively. Moreover, as in a previous report (56), we found that the F-actin arrangement was also disrupted in *Ctnna1*- and *Cdh5*-deficient MLECs (Supplemental Figure 14A, right panel).

Rescue effect of CTNNA1 mutants on AJs and actin filaments of isolated Ctnna1-deficient MLECs. Next, we investigated whether overexpression of WT or *CTNNA1* mutants could rescue disrupted AJs and actin filaments in *Ctnna1*-deficient MLECs. As Supplemental Figure 15 shows, the arrangement of F-actin was well organized in *CTNNA1* WT–transfected *Ctnna1*-deficient MLECs, whereas CTNNA1-P893L and F72S mutant proteins failed to rescue the disrupted F-actin arrangement. Moreover, CTNNA1 WT

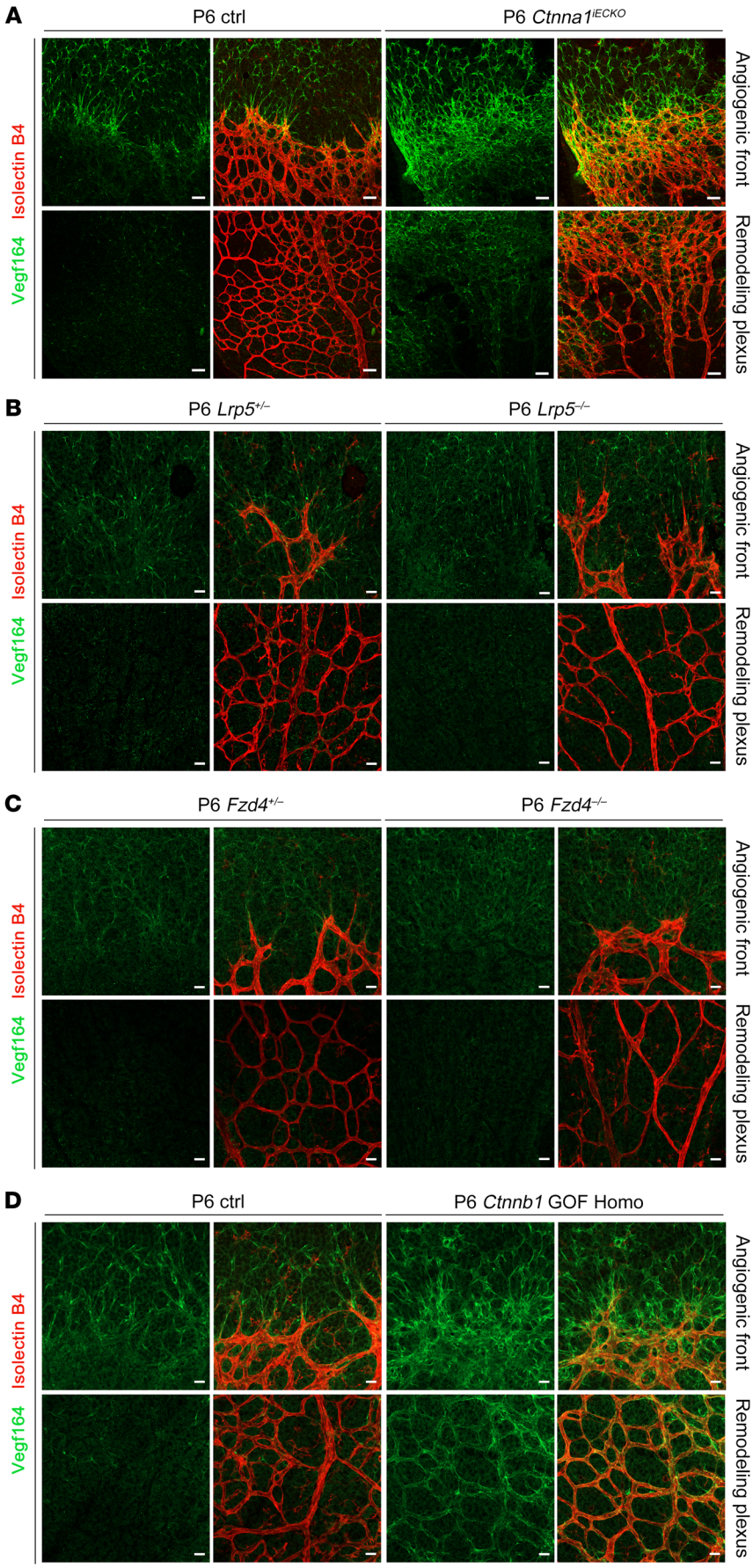

Figure 7. VEGFA distribution in *Ctnna1* endothelial conditional KO, *Lrp5*-KO, *Fzd4*-KO, and *Ctnnb1* GOF Homo mice. (**A**) VEGF164 (green) and IB4 (red) staining of P6 control and $Ctnna1^{iECKO}$ retinas. Abnormal distribution and elevated expression of VEGF164 expressed by both astrocytes and ECs were observed in the angiogenic front and remodeling plexus of $Ctnna1^{iECKO}$ retinal vessels. (**B** and **C**) In P6 $Lrp5^{+/-}$, $Lrp5^{-/-}$, $Fzd4^{+/-}$, and $Fzd4^{-/-}$ retinas, VEGF164 was localized normally in the angiogenic front and absent in the remodeling plexus. Scale bars: 25 μm. (**D**) In P6 control and *Ctnnb1* GOF Homo retinas, abnormal distribution and elevated VEGF164 expression by both astrocytes and ECs were observed in the angiogenic front, whereas in the remodeling plexus, only endothelium-derived VEGF164 expression was elevated. Experiments were performed independently at least 3 times.

protein was able to restore disrupted VE-cadherin and CTNNB1 distribution compared with the vector control. *CTNNA1*-P893L exhibited a compromised ability to rescue compared with *CTNNA1* WT and the vector control. Notably, *CTNNA1*-F72S completely failed to rescue the discontinuous distribution of VE-cadherin and CTNNB1 (Supplemental Figure 15). To explore whether mutations in *CTNNA1* could affect CTNNB1 nuclear translocation, we activated Norrin/β-catenin signaling by adding recombinant Norrin. We found that *CTNNA1* WT protein significantly inhibited the nuclear translocation of CTNNB1 compared with the vector, whereas the mutant forms of CTNNA1 had a compromised inhibitory role in the nuclear translocation of CTNNB1 compared with WT CTNNA1 (Supplemental Figure 16). These data provided additional evidence that CTNNA1 mutants compromised AJs.

The F72S-mutant allele of Ctnna1 combined with the deletion allele of Ctnna1 phenocopy $Ctnna1^{iECKO/iECKO}$ mice. To test whether *Ctnna1* mutation in mice could cause a phenotype similar to that of $Ctnna1^{iECKO/iECKO}$ mice, we generated mice carrying the *Ctnna1*-F72S point mutation. Heterozygous mutant mice ($Ctnna1^{F72S/+}$) were intercrossed to generate homozygous mice, however, we found that the homozygous F72S mutation in the *Ctnna1* gene caused embryonic lethality (Supplemental Table 7). Thus, we examined whether $Ctnna1^{iECKO/F72S}$ compound heterozygous mice exhibited a retinal vascular phenotype similar to that of $Ctnna1^{iECKO/iECKO}$ mice. $Ctnna1^{F72S/+}$ mice were bred with $Ctnnal^{fl/+}$ *Pdgfb-iCre-ER* mice ($Ctnna1^{iECKO/+}$) to generate $Ctnna1^{+/+}$ *Pdgfb-iCre-ER* (control), $Ctnna1^{F72S/+}$, $Ctnnal^{fl/+}$ *Pdgfb-iCre-ER* ($Ctnna1^{iECKO/+}$), and $Ctnna1^{F72S/fl}$ *Pdgfb-iCre-ER* ($Ctnna1^{F72S/iECKO}$)

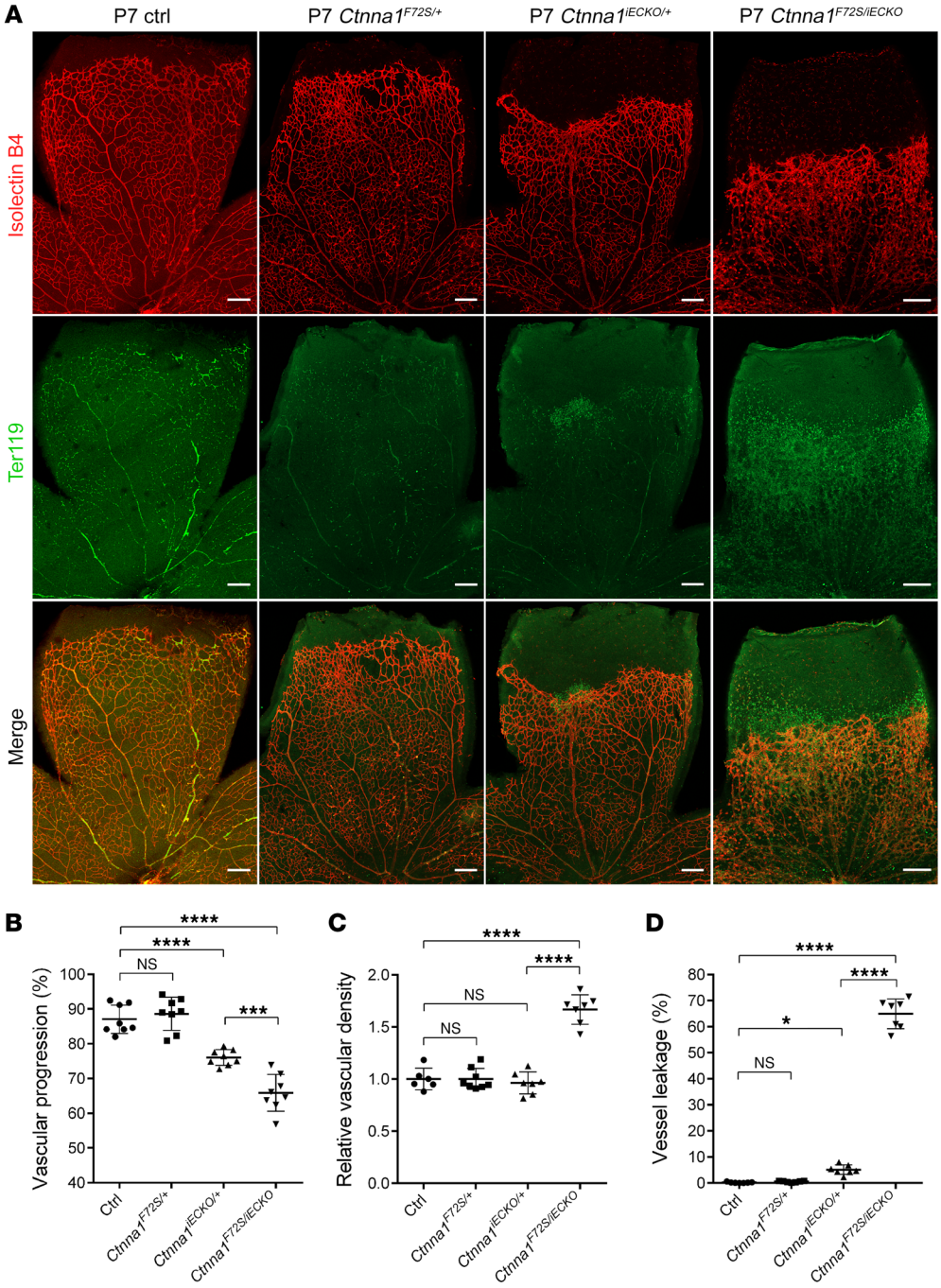

Figure 8. *Ctnna1*$^{F72S/iECKO}$ mice have retinal vasculature similar to that of *Ctnna1*$^{iECKO/iECKO}$ mice. (**A**) Anti-Ter119 (green) and IB4 (red) immunofluorescence staining of retinas from P7 control, *Ctnna1*$^{F72S/+}$, *Ctnna1*$^{iECKO/+}$, and *Ctnna1*$^{F72S/iECKO}$ mice. Scale bars: 200 μm. (**B**–**D**) Quantification of vascular progression, relative vascular density, and vessel leakage. Error bars, SD. $^{*}P < 0.05$, $^{***}P < 0.001$, and $^{****}P < 0.0001$, by 1-way ANOVA with Tukey's multiple-comparison test ($n \geq 6$). Experiments were performed independently at least 3 times.

mice. Confocal images showed that the *F72S* heterozygous mutation could not cause a significant change in vascular development compared with control littermates, whereas the retinal vasculature of *Ctnna1*$^{F72S/iECKO}$ compound heterozygous mice showed retarded growth of horizontal vessels and vessel leakage (Figure 8). This phenotype is similar to that seen in *Ctnna1*$^{iECKO/iECKO}$ mice (Figure 4) and provides another piece of evidence of the pathogenicity of the *CTNNA1-F72S* mutation.

Overactivation of β-catenin signaling results in angiogenesis defects in mouse retinas. Our in vitro cell biology analysis demonstrated that FEVR-associated mutant α-catenin proteins and KD of *CTNNA1* led to increased Norrin/β-catenin activity. These findings suggest that the FEVR phenotype caused by loss of *CTNNA1* function might be partially due to abnormal activation of the Norrin/β-catenin pathway. To investigate whether increased Norrin/β-catenin activity could result in angiogenesis defects, we generated an EC-specific gain-of-function (GOF) allele of *Ctnnb1*. In this allele, exon 3 of *Ctnnb1* was floxed by 2 *loxP* sites (*Ctnnb1*^{floxedexon3}; Supplemental Figure 17A). When this allele was crossed onto a Cre-expressing strain, exon 3 of *Ctnnb1* was deleted in Cre-expressing tissue, abolishing the GSK3β-binding site of β-catenin (Supplemental Figure 17A). This mutant β-catenin protein cannot be degraded by the GSK3β complex, and β-catenin remains activated to drive the expression of its downstream genes. As predicted, we observed β-catenin protein accumulation (220% versus the control) in *Ctnnb1*$^{floxedexon3/floxedexon3}$ *Pdgfb-iCre-ER* (hereafter named *Ctnnb1* GOF Homo) mouse retinal

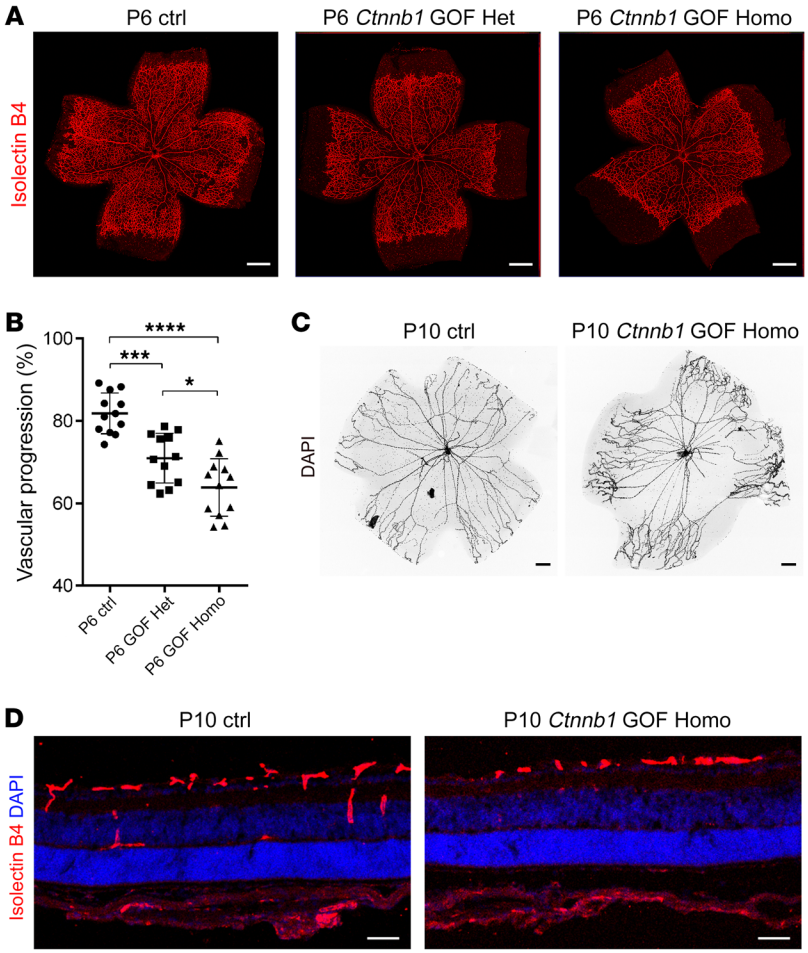

Figure 9. *Ctnnb1* allele GOF in mice causes retinal vascularization defects. (**A**) P6 flat-mounted retinas from control, *Ctnnb1*$^{floxedexon3/+}$ *Pdgfb-iCre-ER* heterozygous (*Ctnnb1* GOF Het), and *Ctnnb1*$^{floxedexon3/floxedexon3}$ *Pdgfb-iCre-ER* homozygous (*Ctnnb1* GOF Homo) mice were stained with IB4. Compared with those of littermate controls, retinas from the heterozygous *Ctnnb1* GOF and homozygous *Ctnnb1* GOF mice showed incomplete retinal vascularization. Scale bars: 500 μm. (**B**) Quantification of vascular progression at P6. Error bars indicate the SD. **P* < 0.05, ****P* < 0.001, and *****P* < 0.0001, by 1-way ANOVA with Tukey's multiple-comparison test (*n* = 12). (**C**) DAPI staining of hyaloid vessels in the eyes of control and *Ctnnb1* GOF Homo mice, showing relatively delayed hyaloid vessel regression in the eyes of *Ctnnb1* GOF Homo mice. Scale bars: 250 μm. (**D**) Frozen retinal sections from P9 control and *Ctnnb1* GOF Homo mice were costained with IB4 (red) and DAPI (blue). Scale bars: 25 μm. Experiments were performed independently at least 3 times.

ECs (Supplemental Figure 17, B and C). Expression of this *Ctnnb1* GOF allele in mouse ECs resulted in retarded superior retinal blood vessel growth and defects in vertical vascular growth into the deeper retinal layers, with secondary and tertiary vessels absent at P9 (Figure 9), which is similar to some clinical features of FEVR (3–5, 7, 12, 24, 25). However, the retinal vasculature of P13 *Ctnnb1* GOF Homo mice only showed mild retarded growth into deep vessel layers (Supplemental Figure 18), indicating that overactivation of β-catenin signaling could partially affect vessel development. Furthermore, as in *Ctnna1*$^{iECKO/iECKO}$, upregulation of VEGFA and DLL4 was also observed in *Ctnnb1* GOF Homo retinas (Figure 7D and Supplemental Figure 9). These findings demonstrated that β-catenin activity has to be maintained in a precise range and that increased β-catenin activity can disrupt angiogenesis in the retina (3–5, 7, 12, 24, 25).

During WES analysis, we also identified a missense mutation (p.P848L) in the *LRP5* gene that led to a 2-fold increase of Norrin/β-catenin signaling luciferase activity in an Indian family with FEVR (Supplemental Figure 19). We then generated an *Lrp5*^{P847L}-knockin (*Lrp5*^{P847L}-KI) mouse corresponding to the *LRP5*-848L human mutation to examine its effect on retinal angiogenesis. The *Lrp5*-KI allele led to retarded angiogenesis, as seen in the *Ctnnb1* GOF Homo mice and similar to phenotypes observed in patients with FEVR (Figure 10 and Supplemental Figure 20). This evidence provides further support for the role of increased β-catenin activity in FEVR pathogenesis without affecting the maintenance of barrier function.

Discussion

It is established that approximately half of patients with FEVR have mutations in *NDP*, *FZD4*, *LRP5*, and *TSPAN12*, which encode components of the Norrin/β-catenin pathway (3–5, 7, 12, 24, 25) through inactivation of Norrin/β-catenin signaling. In this study, we demonstrated that mutations in *CTNNA1* in the cadherin-catenin complex caused FEVR through overactivation of Norrin/β-catenin signaling and interruption of cell junctions, suggesting that the cadherin-catenin complex plays an important role in the pathogenesis of FEVR. Mutations in *CTNNA1* result in reduced sequestration of β-catenin in the cytosol and increased activity of Norrin/β-catenin signaling. Consistent with this finding, mutations in *CTNNB1*, which encodes a core member of the cadherin-catenin complex and functions as a key effector in the Norrin/β-catenin pathway, were recently reported to be associated with FEVR, further supporting a role for the cadherin-catenin complex in the etiology of these retinal diseases (11, 12). Two types of mutations have recently been identified in *CTNNB1*, one that decreases β-catenin activity and one that increases β-catenin activity (12), indicating that the transcriptional activity of *CTNNB1* has to be maintained within a narrow range. These findings, together with our results showing that transcriptional activity of β-catenin protein must be precisely regulated within a narrow window to maintain proper vessel development, suggest that β-catenin plays a central role in merging the cadherin/β-catenin

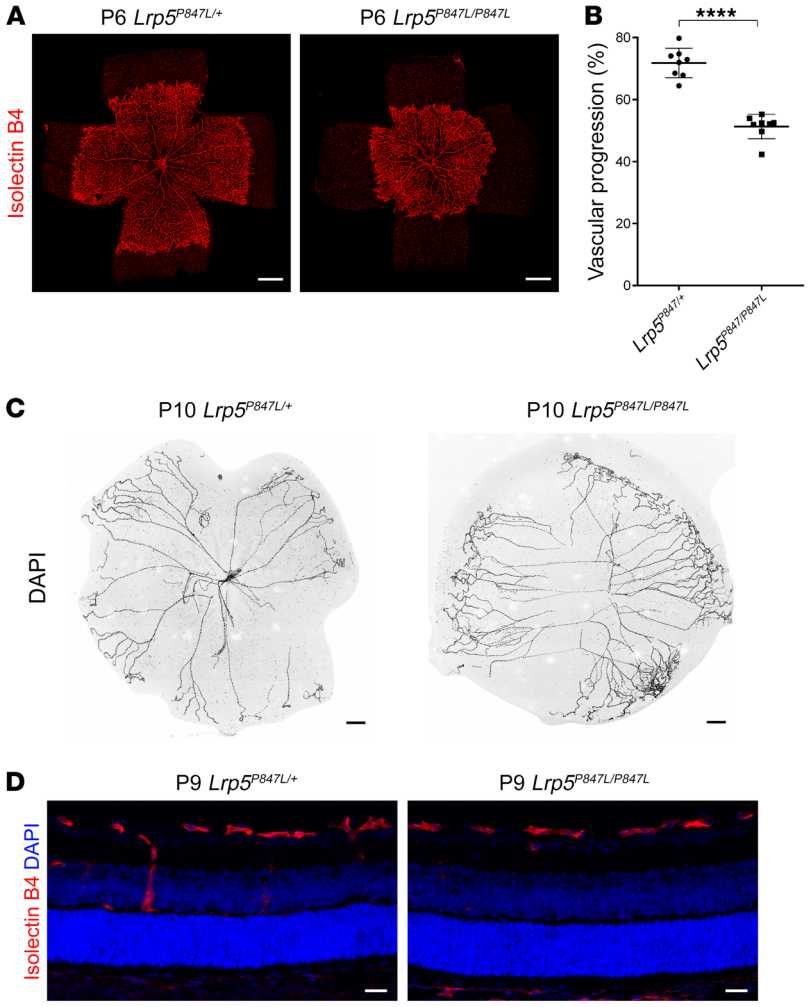

Figure 10. Mutation of *Lrp5 P847L* in mice causes retinal vascularization defects. (**A**) Images of P6 flat-mounted, IB4-stained retinas from $Lrp5^{P847L/+}$ and $Lrp5^{P847L/P847L}$ mice. Compared with those of $Lrp5^{P847L/+}$ mice, retinas from $Lrp5^{P847L/P847L}$ mice showed incomplete vascularization. Scale bars: 500 μm. (**B**) Quantification of the vascular progression in retinas from $Lrp5^{P847L/+}$ and $Lrp5^{P847L/P847L}$ mice on P6. Error bars indicate the SD. $^{****}P < 0.0001$, by Student's *t* test ($n = 8$). (**C**) DAPI staining of hyaloid vessels in the eyes of $Lrp5^{P847L/+}$ and $Lrp5^{P847L/P847L}$ mice, showing delayed hyaloid vessel regression in the eyes of $Lrp5^{P847L/P847L}$ mice. Scale bars: 250 μm. (**D**) Frozen retinal sections from P9 $Lrp5^{P847L/+}$ and $Lrp5^{P847L/P847L}$ mice were costained with IB4 (red) and DAPI (blue). Scale bars: 25 μm. Experiments were performed independently at least 3 times.

and Norrin/β-catenin pathways, making it a pivotal protein in the pathogenesis of FEVR.

Previous studies have indicated that dysfunction of *CTNNA1* could result in cancer and developmental diseases (57). However, we did not found cancer in our affected patients. Following American College of Medical Genetics and Genomics (ACMG) guidelines (58, 69), we referred the patient with p.R376Cfs*27 for genetic counseling. Recently, Saksens et al. identified 3 heterozygous missense mutations in *CTNNA1* (c.953T>C, p.Leu318Ser; c.1293T>G, p.Ile431Met; and c.919G>A, p.Glu307Lys) in patients with butterfly macular dystrophy (35). Notably, another *CTNNA1* variant (c.160C>T; p.Arg54Cys) was identified in a patient with butterfly-shaped pigment dystrophy (35) and in a patient with AMD who lacked the classical butterfly-shaped pigment dystrophy phenotype (36). The pathogenicity of this variant remains unclear. Alexander, et al. (37) recently identified 4 missense mutations in *CTNNA1* (c.965C>T, p.Ser322Leu; c.1316C>T, p.Ser439Phe; c.1294G>A, p.Glu432Lys; and c.973A>G, p.Thr325Ala) in patients with macular pattern dystrophy. These identified variants were predicted by the SIFT (sorting intolerant from tolerant) program to be disease causing and to affect a residue that is completely conserved among vertebrate species. A chemically induced $Ctnna1^{tvrm5}$ mouse model exhibited similar pigmentary abnormalities, focal thickening, and elevated lesions, as well as decreased light-activated electroretinographic (ERG) responses and loss of photoreceptor cells, and carried the homozygous missense mutation *Ctnna1* p.Leu436Pro (35). According to an x-ray crystallographic structural model of the human CTNNA1 protein (Protein Data Bank [PDB]: 4IGG; Supplemental Figure 22A and ref. 60), residues affected by those 4 variants associated with butterfly macular dystrophy (p.Glu307, p.Leu318, p.Ile431, and p.Leu436; ref. 35) and 4 variants with macular pattern dystrophy (p.Ser322, p.Ser439, p.Glu432, and Thr325; ref. 37) are located close to one another in the force-sensing module (domains D3–D4, amino acid residues 260–630) and in protein-binding domains (D3a, residues 260–400; D3b, residues 400–507), suggesting that mutations in these domains might lead to macular dystrophy. The 2 missense *CTNNA1* mutations associated with FEVR identified in our study are located near distinct helix bundles (p.Phe72 in the N-terminal helix and p.Pro893 in the C-terminal helix, respectively) in the crystal structure, and these 2 helix bundles (hereafter referred to as helix-N and helix-C) are spatially close (Supplemental Figure 22A). Furthermore, structural analysis of CTNNA1 asymmetric dimers (chain A and chain B) revealed that the helix-N of chain A was spatially closer to the helix-C of chain B than to the helix-N of chain B (Supplemental Figure 22B), indicating that Phe72 and Pro893 residues might partic-

ipate in similar functions. This was also supported by our data that both variants affected F-actin orientation (Figure 2E and Supplemental Figure 15) and partially lost the ability to inhibit β-catenin signaling (Figure 2B and Supplemental Figures 1 and 16). It is plausible that different *CTNNA1* variants have different effects on the protein functions and lead to distinct disease conditions. Another similar example is the FEVR disease–causing gene *LRP5*. Mutations in *LRP5* resulted in osteopenia and osteoporosis (18), whereas distinct mutations in *LRP5* also caused FEVR (4).

KD of *CTNNA1* in HRECs resulted in dissociated AJ proteins of the cadherin-catenin complex (Figure 3), such as VE-cadherin (*CDH5*), β-catenin (*CTNNB1*), and δ-catenin (*CTNND1*), on the cell membrane. F-actin was disorganized in HRECs expressing the mutant CTNNA1 proteins and in *CTNNA1*-KD cells, indicating that functional disruption of *CTNNA1* damages the actin cytoskeleton network. Although CTNNA1-P893L might not affect its binding with CTNNB1 and cell localization like CTNNA1-F72S does (Figure 2A), this mutant protein indeed disrupts the F-actin network (Figure 2E) and activates β-catenin signaling compared with WT CTNNA1 (Figure 2B), suggesting that the F-actin network might play a role in retinal vascular development. In addition, in our rescue experiment using an adenovirus, both CTNNA1-P893L– and F72S-mutant proteins failed to rescue the disrupted F-actin arrangement and the VE-cadherin and CTNNB1 distribution in isolated MLECs (Supplemental Figures 15 and 16). However, the exact mechanism by which P893L mutation causes FEVR remains elusive and needs further investigation.

The crucial role of *CTNNA1* in the pathogenesis of FEVR is strongly supported by the retinal blood vessel phenotypes observed in the *Ctnna1* EC–specific KO mouse model. Both $Ctnna1^{iECKO/+}$ and $Ctnna1^{iECKO/iECKO}$ mice showed incomplete vascularization of the peripheral retina, an absence of the secondary and tertiary capillary layers in the deep retina, delayed hyaloid vasculature regression, and vascular leakage in the retina (Figure 4), reproducing the main clinical features of patients with FEVR. It is true that the $Ctnnal^{iECKO/+}$ model had only a milder phenotype than what was observed in patients with FEVR. This might be due to a species difference. Another similar example is the *Lrp5*- or *Fzd4*-KO model for FEVR. *Lrp5* or *Fzd4* heterozygous KO mice showed no visible angiogenesis defects, but homozygous KO mice exhibited FEVR-like phenotypes (24, 25). In contrast to *Lrp5*- and *Fzd4*-KO models with inactivation of β-catenin signaling, loss of *Ctnna1* in $Ctnna1^{iECKO/iECKO}$ retinas resulted in overactivation of β-catenin signaling, disruption of the VEGFA gradient (Figure 7), and drastic upregulation of the notch ligand DLL4 (Supplemental Figure 9). Abnormal distribution of VEGFA in the remodeling plexus might result in a high density of blood vessels in retinas. Consequently, both *CTNNA1*-KD HRECs and $Ctnna1^{iECKO/iECKO}$ retinal ECs exhibited increased proliferation, possibly induced by overactivation of β-catenin signaling and vascular leakage–associated upregulation of VEGFA (Figures 5 and 7 and Supplemental Figure 3). DLL4 plays an inhibitory role in tip cell formation and promotes stalk cell differentiation (61). A high concentration of DLL4 might inhibit radial growth of the retinal vasculature (61, 62). Constitutive activation of β-catenin in *Ctnnb1* GOF also led to upregulation of the notch ligand DLL4 (Supplemental Figure 9). These results demonstrate that the transcriptional activity of β-catenin protein has to be precisely regulated within a narrow window to maintain proper vessel development.

$Ctnna1^{iECKO}$ retinas exhibited increased proliferation and delayed vascular expansion. This paradox can be explained by the following 2 factors. First, tip cell migration depends on a normal VEGF gradient (51). Loss of *Ctnna1* led to activation of β-catenin signaling and disruption of the normal VEGFA gradient, because increased expression of VEGFA was observed in both the remodeling plexus and angiogenic front of the retina (Figure 7A). This abnormal VEGFA gradient resulted in excessive angiogenesis in the remodeling plexus rather than vascular expansion. Second, binding of CTNNA1 with vinculin was previously reported to be crucial for maintaining migration polarity in ECs (63), and loss of *Ctnna1* in mouse ECs might impair collective polarity, leading to deficient outward angiogenesis.

The cadherin-catenin complex plays a critical role in cellular AJs and maintains the integrity of cell-cell connections (64). In the cadherin-catenin complex, VE-cadherin interacts with several binding partners, such as α-catenin, β-catenin, and p120-catenin, to maintain normal cell-cell adherens and dynamics (65). Dysfunction of AJs might result in vascular diseases (66), and, indeed, VE-cadherin/β-catenin signaling controls vascular EC survival (42). A recent study by Yamamoto et al., combined with our work (Supplemental Figure 13), found hemorrhaging in the peripheral retina, incomplete retina vascular development, defective sprouting into the deeper retina, and local hyperdensity of the retinal vasculature near the angiogenic front in $Cdh5^{iECKO/iECKO}$-mutant mice (54, 55). These retinal vascular development defects reproduce the main clinical phenotypes of FEVR, supporting the hypothesis that disruption of the cadherin-catenin complex causes FEVR.

In contrast to the previously reported role of *NDP*, *FZD4*, *LRP5*, and *TSPAN12* mutations in decreasing Norrin/β-catenin signaling (3–5, 7, 12, 24, 25), we observed that FEVR-causing *CTNNA1* mutations overactivated Norrin/β-catenin signaling. In addition, it is interesting that we identified a FEVR-causing *LRP5* mutation with increased Norrin/β-catenin transcriptional activity, in contrast to the loss-of-function *LRP5* mutations identified in patients with FEVR (4, 5). Consistent with this finding, a recent study reported that a FEVR-associated *CTNNB1* mutation (p.R710C) increased the transcriptional activity of Norrin/β-catenin as well as a loss-of-function mutation (p.H720*; ref. 12), suggesting that overactivation of Norrin/β-catenin is associated with FEVR. In addition, overactivation of Norrin/β-catenin signaling by the overexpression of Norrin in transgenic mice disrupted embryonic angiogenesis (25), further supporting our hypothesis that overactivation of Norrin/β-catenin signaling could cause defective angiogenesis. Importantly, we demonstrated that mice expressing an EC-specific GOF of the *Ctnnb1* allele exhibited the main FEVR phenotypes, including an incomplete vascularization of the peripheral retina and a lack of secondary and tertiary capillary layers in the deep retina (Figure 9). It thus appears that precisely controlled β-catenin activation is critical for normal retinal vascular development. Both the loss of β-catenin activity, caused by mutations in the *NDP/FZD4/LRP5/TSPAN12/CTNNB1* pathway, and the overactivation of β-catenin activity via mutations in the *CTNNA1-CTNNB1* complex are associated with FEVR. Notably, the development of vascular defects in the GOF allele of *Ctnnb1* and $Lrp5^{P847L/P847L}$ mice was much milder

than that observed in *Ctnna1*$^{iECKO/iECKO}$ mice (Figures 4, 9, and 10 and Supplemental Figures 5, 18, and 21), possibly because overactivation of β-catenin has a limited effect on vascular development.

On the basis of our observation of AJ defects in *CTNNA1*-depleted HRECs, we propose that dysfunction of the cadherin-catenin complex and excessive β-catenin transcriptional activity could cause FEVR pathogenesis. In fact, similar to the phenotypes of *Fzd4* and *Lrp5* homozygous KO mutants, loss of *Ctnna1* in ECs resulted in an abnormal proliferation of ECs (Figure 6), extensive leakage in retinal vessels (Figure 4, F and I), retarded radical growth, a lack of capillary layers in the deep retina, and delayed hyaloid vasculature regression, which were also observed in the retinas of mice with the *Ctnnb1* or *Lrp5*^{P847L} GOF allele (Figures 4, 9, and 10). Thus, this study not only provides new insight into the pathogenesis and therapeutic targets of FEVR, but also sheds light on pathogenesis clues for other blindness diseases accompanied by neovascularization. A future challenge will be to determine precisely how altered cadherin-catenin complex function and overactivated Norrin/β-catenin independently contribute to the pathogenesis of FEVR and other neovascularization blindness diseases.

Taken together, these findings demonstrate that dysfunction of the cadherin-catenin complex and dysregulation of Norrin/β-catenin transcriptional activity are of key importance for the development of FEVR and potentially other neovascular diseases. Of course, our finding is tentative and would benefit from replication in other cohorts and FEVR families.

Methods

A full description of the methods is provided in the Supplemental Methods.

WES. Exome sequencing was performed on DNA samples from the index patients. The raw sequence data reported in this study have been deposited in the Genome Sequence Archive of the National Genomics Data Center (NGDC) (67), Beijing Institute of Genomics (China National Center for Bioinformation), Chinese Academy of Sciences (accession no. HRA000554; https://bigd.big.ac.cn/gsa).

Experimental animals. All mice were on a C57BL/6 background. Mice were housed under a 12-hour light/12-hour dark cycle at 25°C and had unrestricted access to food and water.

Floxed *Ctnnal* mice were obtained from The Jackson Laboratory (stock no. 004604; https://www.jax.org/strain/004604; ref. 68). *Ctnna1*$^{fl/fl}$ mice were mated with *Pdgfb-iCre*–transgenic mice (69) to generate *Ctnna1*$^{iECKO/iECKO}$ mice with inducible alleles to inactivate *Ctnna1* in ECs. To monitor the efficiency of the Cre-mediated deletion of the floxed *Ctnna1* exon, a tdTomato reporter was used (stock no. 007914; strain name: B6.Cg-Gt [ROSA] 26Sortm14 [CAG-tdTomato]Hze/J, also named Ai14D, http://jaxmice.jax.org/strain/007914.html) (70). The reporter contained a *loxP*-flanked STOP cassette that prevented the transcription of the downstream CAG promoter–driven red fluorescent protein variant tdTomato. The STOP cassette was removed in the Cre-expressing tissue(s), and tdTomato was expressed. Because this CAG promoter–driven reporter construct was inserted into the Gt (ROSA) 26Sor locus, tdTomato was expressed only in tissues that expressed Cre.

Floxed *Cdh5* mice were obtained from Cyagen (https://www.cyagen.com/cn/zh-cn/sperm-bank-cko/12562). *Lrp5*-KO mice were obtained from The Jackson Laboratory (stock no. 005823, https://www.jax.org/strain/005823). *Fzd4*-KO mice were obtained from The Jackson Laboratory (stock no. 012823, https://www.jax.org/strain/012823). *Ctnnb1*$^{floxedexon3/+}$ mice were generated by ViewSolid Biotech using the CRISPR/Cas9 nickase technique via a design described by Harada et al. (71). Two *loxP* sites with the same orientation were placed upstream and downstream of exon 3 of the *Ctnnb1* gene. *Ctnnb1*$^{fledExon3/+}$ mice were mated with *Pdgfb-iCre*–transgenic mice (69) to generate *Ctnnb1*$^{floxedexon3/+}$ *Pdgfb-iCre-ER* mice.

Ctnna1 F72S–KI mice carrying the F72S mutation corresponding to the human F72S mutation (named *Ctnna1*^{em1XJZ}, hereafter referred to as *Ctnna1*^{F72S}) were generated using the CRISPR/Cas9 nickase technique. The genomic RNA (gRNA) sequence was as follows: AAGCAACTGAGAATTTCTTGG. The donor oligo with the sequence CCATGTTTTGGCTGCATCTGTTGAACAAGCAACTGAGAATTCCTTGGAAAAGGGGGATAAAATTGCAAAAGAGAGCCAGT was coinjected into the C57BL/6J zygotes to introduce a F72S point mutation into the mouse genome. The *Ctnna1*^{F72S}-targeting allele was screened using a sequencing PCR product.

Lrp5-KI mice carrying the P847L mutation corresponding to the human P848L mutation (named *Lrp5*^{em1XJZ} and hereafter referred to as *Lrp5*^{P847L} mice) were generated using the CRISPR/Cas9 nickase technique. the gRNA sequence was as follows: GACGATCTGCCCTACCCGTTTGG. Donor oligonucleotides with the sequence TATGTGCTATGTCCCCGCACAGGTCAGGAGCGCATGGTGATAGCTGACGATCTGCCCTACTGTTTGGCCTGACTCAATATAGCGATTACATCTACTGGACTGACTGGAACCTGCATAGCATT were coinjected into C57BL/6J zygotes to introduce the P847L point mutation into the mouse genome. The *Lrp5*^{P847L}-targeting allele was screened using a sequencing PCR product.

Western blot analysis. The primary and secondary antibodies used for Western blotting are listed in Supplemental Table 12. Uncropped immunoblots are shown in the supplemental material.

Statistics. All data are presented as the mean ± SD. Animals were assigned randomly to experimental groups. Western blotting signals were detected using Image Quant LAS 500 (GE Life Sciences), and ImageJ software (NIH) was used to quantify the detected signals. Statistical analysis was performed with GraphPad Prism 6.0 (GraphPad Software). The data sets were tested for normal distribution using the Shapiro-Wilk test. If the data set was not normally distributed, a nonparametric statistics was used. *P* values were calculated with a 2-tailed Student's *t* test or a 1- or 2-way ANOVA followed by Tukey's, Dunnett's, or Sidak's multiple-comparison test as appropriate. A *P* value of less than 0.05 was considered statistically significant.

Study approval. This research was carried out in accordance with the tenets of the Declaration of Helsinki and was approved by the ethics oversight committee of Sichuan Provincial People's Hospital, Xinhua Hospital, Shanghai Jiaotong University, and the Aravind Eye Hospital. Written informed consent was obtained from all participants in this study or from the legal guardians of minors. All animal protocols were approved by the IACUC of Sichuan Provincial People's Hospital. All experimental procedures and methods were performed in accordance with the approved study protocols and relevant regulations.

Author contributions

ZY and Xianjun Zhu designed and supervised the study. PZ, Xiong Zhu, Xiang Zhang , PF, and PS recruited the participants. LH and ZY performed the sequencing analysis. Xianjun Zhu, SL, MY, LZ,

WZ, and ZY performed the animal analysis, cell biology, immunohistochemistry, and gene expression studies. LZ, YH, Y. Yang, Y. Yuan, Xiong Zhu, SZ, and HX performed the construction and mutation of plasmids. SM and FH were responsible for sample preservation and DNA extraction. SZ, Xiong Zhu, and HX were responsible for animal breeding. Xianjun Zhu, MY, SL, and ZY wrote the manuscript. All authors critically revised and gave final approval to this manuscript.

Acknowledgments

The authors want to thank all the patients and their family members for participating in this study. This research project was supported by the National Precision Medicine Project (2016YFC0905200), the National Natural Science Foundation of China (81790643, to ZY; 81970841 and 81770950, to Xianjun Zhu; 82000913, to SL; 82071009, to LZ; 81770964 and 81470642, to PZ; 81770963, to PF; 81670895, to LH); the Chinese Academy of Medical Sciences (CAMS) Innovation Fund for Medical Sciences (2019-12M-5-032); the Department of Science and Technology of Sichuan Province of China (2020ZYD037, to ZY; 20YZHY0011, to Xianjun Zhu; 2017JQ0024 and 2016HH0072, to LH; 2018YSZH0020, to LZ; and 2019M653382, to SL).

Address correspondence to: Zhenglin Yang, Sichuan Provincial Key Laboratory for Human Disease Gene Study, Sichuan Provincial People's Hospital, University of Electronic Science and Technology of China, 32 The First Ring Road West 2, Chengdu, Sichuan 610072, China. Phone: 86.28.8739.3375; Email: zliny@yahoo.com.

1. Criswick VG, Schepens CL. Familial exudative vitreoretinopathy. *Am J Ophthalmol*. 1969;68(4):578–594.
2. Collin RW, et al. ZNF408 is mutated in familial exudative vitreoretinopathy and is crucial for the development of zebrafish retinal vasculature. *Proc Natl Acad Sci U S A*. 2013;110(24):9856–9861.
3. Robitaille J, et al. Mutant frizzled-4 disrupts retinal angiogenesis in familial exudative vitreoretinopathy. *Nat Genet*. 2002;32(2):326–330.
4. Toomes C, et al. Mutations in LRP5 or FZD4 underlie the common familial exudative vitreoretinopathy locus on chromosome 11q. *Am J Hum Genet*. 2004;74(4):721–730.
5. Jiao X, et al. Autosomal recessive familial exudative vitreoretinopathy is associated with mutations in LRP5. *Am J Hum Genet*. 2004;75(5):878–884.
6. Chen ZY, et al. A mutation in the Norrie disease gene (NDP) associated with X-linked familial exudative vitreoretinopathy. *Nat Genet*. 1993;5(2):180–183.
7. Junge HJ, et al. TSPAN12 regulates retinal vascular development by promoting Norrin- but not Wnt-induced FZD4/beta-catenin signaling. *Cell*. 2009;139(2):299–311.
8. Nikopoulos K, et al. Next-generation sequencing of a 40 Mb linkage interval reveals TSPAN12 mutations in patients with familial exudative vitreoretinopathy. *Am J Hum Genet*. 2010;86(2):240–247.
9. Poulter JA, et al. Mutations in TSPAN12 cause autosomal-dominant familial exudative vitreoretinopathy. *Am J Hum Genet*. 2010;86(2):248–253.
10. Robitaille JM, et al. Phenotypic overlap between familial exudative vitreoretinopathy and microcephaly, lymphedema, and chorioretinal dysplasia caused by KIF11 mutations. *JAMA Ophthalmol*. 2014;132(12):1393–1399.
11. Dixon MW, et al. CTNNB1 mutation associated with familial exudative vitreoretinopathy (FEVR) phenotype. *Ophthalmic Genet*. 2016;37(4):468–470.
12. Panagiotou ES, et al. Defects in the cell signaling mediator β-catenin cause the retinal vascular condition FEVR. *Am J Hum Genet*. 2017;100(6):960–968.
13. Khan K, et al. Next generation sequencing identifies mutations in Atonal homolog 7 (ATOH7) in families with global eye developmental defects. *Hum Mol Genet*. 2012;21(4):776–783.
14. Wu JH, et al. Haploinsufficiency of RCBTB1 is associated with Coats disease and familial exudative vitreoretinopathy. *Hum Mol Genet*. 2016;25(8):1637–1647.
15. Downey LM, et al. A new locus for autosomal dominant familial exudative vitreoretinopathy maps to chromosome 11p12-13. *Am J Hum Genet*. 2001;68(3):778–781.
16. Park H, et al. Integrin-linked kinase controls retinal angiogenesis and is linked to Wnt signaling and exudative vitreoretinopathy. *Nat Commun*. 2019;10(1):5243.
17. Zhang L, et al. Exome sequencing revealed Notch ligand JAG1 as a novel candidate gene for familial exudative vitreoretinopathy. *Genet Med*. 2020;22(1):77–84.
18. Gong Y, et al. LDL receptor-related protein 5 (LRP5) affects bone accrual and eye development. *Cell*. 2001;107(4):513–523.
19. Berger W, et al. Isolation of a candidate gene for Norrie disease by positional cloning. *Nat Genet*. 1992;1(3):199–203.
20. Ostergaard P, et al. Mutations in KIF11 cause autosomal-dominant microcephaly variably associated with congenital lymphedema and chorioretinopathy. *Am J Hum Genet*. 2012;90(2):356–362.
21. Tucci V, et al. Dominant β-catenin mutations cause intellectual disability with recognizable syndromic features. *J Clin Invest*. 2014;124(4):1468–1482.
22. Li VS, et al. Wnt signaling through inhibition of β-catenin degradation in an intact Axin1 complex. *Cell*. 2012;149(6):1245–1256.
23. Smallwood PM, et al. Mutational analysis of Norrin-frizzled4 recognition. *J Biol Chem*. 2007;282(6):4057–4068.
24. Xu Q, et al. Vascular development in the retina and inner ear: control by Norrin and Frizzled-4, a high-affinity ligand-receptor pair. *Cell*. 2004;116(6):883–895.
25. Ye X, et al. Norrin, frizzled-4, and Lrp5 signaling in endothelial cells controls a genetic program for retinal vascularization. *Cell*. 2009;139(2):285–298.
26. Gilmour DF. Familial exudative vitreoretinopathy and related retinopathies. *Eye (Lond)*. 2015;29(1):1–14.
27. Salvo J, et al. Next-generation sequencing and novel variant determination in a cohort of 92 familial exudative vitreoretinopathy patients. *Invest Ophthalmol Vis Sci*. 2015;56(3):1937–1946.
28. Kobielak A, Fuchs E. Alpha-catenin: at the junction of intercellular adhesion and actin dynamics. *Nat Rev Mol Cell Biol*. 2004;5(8):614–625.
29. Piao HL, et al. α-catenin acts as a tumour suppressor in E-cadherin-negative basal-like breast cancer by inhibiting NF-κB signalling. *Nat Cell Biol*. 2014;16(3):245–254.
30. Liu TX, et al. Chromosome 5q deletion and epigenetic suppression of the gene encoding alpha-catenin (CTNNA1) in myeloid cell transformation. *Nat Med*. 2007;13(1):78–83.
31. Ji H, et al. α-Catenin inhibits glioma cell migration, invasion, and proliferation by suppression of β-catenin transactivation. *J Neurooncol*. 2011;103(3):445–451.
32. Silvis MR, et al. α-catenin is a tumor suppressor that controls cell accumulation by regulating the localization and activity of the transcriptional coactivator Yap1. *Sci Signal*. 2011;4(174):ra33.
33. Buckley CD, et al. Cell adhesion. The minimal cadherin-catenin complex binds to actin filaments under force. *Science*. 2014;346(6209):1254211.
34. Majewski IJ, et al. An α-E-catenin (CTNNA1) mutation in hereditary diffuse gastric cancer. *J Pathol*. 2013;229(4):621–629.
35. Saksens NT, et al. Mutations in CTNNA1 cause butterfly-shaped pigment dystrophy and perturbed retinal pigment epithelium integrity. *Nat Genet*. 2016;48(2):144–151.
36. de Breuk A, et al. Development of a genotype assay for age-related macular degeneration: the EYE-RISK Consortium [published online July 25, 2020]. *Ophthalmology*. https://doi.org/10.1016/j.ophtha.2020.07.037.
37. Tanner A, et al. Clinical and genetic findings in CTNNA1-associated macular pattern dystrophy [published online November 1, 2020]. *Ophthalmology*. https://doi.org/10.1016/j.ophtha.2020.10.032.
38. Gong B, et al. Mutant RAMP2 causes primary open-angle glaucoma via the CRLR-cAMP axis. *Genet Med*. 2019;21(10):2345–2354.
39. Novarino G, et al. Exome sequencing links corticospinal motor neuron disease to com-

mon neurodegenerative disorders. *Science*. 2014;343(6170):506–511.
40. Drees F, et al. Alpha-catenin is a molecular switch that binds E-cadherin-beta-catenin and regulates actin-filament assembly. *Cell*. 2005;123(5):903–915.
41. Yamada S, et al. Deconstructing the cadherin-catenin-actin complex. *Cell*. 2005;123(5):889–901.
42. Carmeliet P, et al. Targeted deficiency or cytosolic truncation of the VE-cadherin gene in mice impairs VEGF-mediated endothelial survival and angiogenesis. *Cell*. 1999;98(2):147–157.
43. Hwang SG, et al. Regulation of β-catenin signaling and maintenance of chondrocyte differentiation by ubiquitin-independent proteasomal degradation of α-catenin. *J Biol Chem*. 2005;280(13):12758–12765.
44. Simcha I, et al. Differential nuclear translocation and transactivation potential of beta-catenin and plakoglobin. *J Cell Biol*. 1998;141(6):1433–1448.
45. Takahashi N, et al. Posttranscriptional regulation of alpha-catenin expression is required for Wnt signaling in L cells. *Biochem Biophys Res Commun*. 2000;277(3):691–698.
46. Su W, Kowalczyk AP. The VE-cadherin cytoplasmic domain undergoes proteolytic processing during endocytosis. *Mol Biol Cell*. 2017;28(1):76–84.
47. Luhmann UF, et al. Role of the Norrie disease pseudoglioma gene in sprouting angiogenesis during development of the retinal vasculature. *Invest Ophthalmol Vis Sci*. 2005;46(9):3372–3382.
48. Lobov IB, et al. WNT7b mediates macrophage-induced programmed cell death in patterning of the vasculature. *Nature*. 2005;437(7057):417–421.
49. Wang Y, et al. Norrin/Frizzled4 signaling in retinal vascular development and blood brain barrier plasticity. *Cell*. 2012;151(6):1332–1344.
50. del Toro R, et al. Identification and functional analysis of endothelial tip cell-enriched genes. *Blood*. 2010;116(19):4025–4033.
51. Gerhardt H, et al. VEGF guides angiogenic sprouting utilizing endothelial tip cell filopodia. *J Cell Biol*. 2003;161(6):1163–1177.
52. Jakobsson L, et al. Endothelial cells dynamically compete for the tip cell position during angiogenic sprouting. *Nat Cell Biol*. 2010;12(10):943–953.
53. Zhou Z, et al. Cerebral cavernous malformations arise from endothelial gain of MEKK3-KLF2/4 signalling. *Nature*. 2016;532(7597):122–126.
54. Gaengel K, et al. The sphingosine-1-phosphate receptor S1PR1 restricts sprouting angiogenesis by regulating the interplay between VE-cadherin and VEGFR2. *Dev Cell*. 2012;23(3):587–599.
55. Yamamoto H, et al. Integrin β1 controls VE-cadherin localization and blood vessel stability. *Nat Commun*. 2015;6:6429.
56. Lampugnani MG, et al. VE-cadherin regulates endothelial actin activating Rac and increasing membrane association of Tiam. *Mol Biol Cell*. 2002;13(4):1175–1189.
57. Ding L, et al. Genome remodelling in a basal-like breast cancer metastasis and xenograft. *Nature*. 2010;464(7291):999–1005.
58. Green RC, et al. ACMG recommendations for reporting of incidental findings in clinical exome and genome sequencing. *Genet Med*. 2013;15(7):565–574.
59. Kalia SS, et al. Recommendations for reporting of secondary findings in clinical exome and genome sequencing, 2016 update (ACMG SF v2.0): a policy statement of the American College of Medical Genetics and Genomics. *Genet Med*. 2017;19(2):249–255.
60. Rangarajan ES, Izard T. Dimer asymmetry defines α-catenin interactions. *Nat Struct Mol Biol*. 2013;20(2):188–193.
61. Benedito R, et al. The notch ligands Dll4 and Jagged1 have opposing effects on angiogenesis. *Cell*. 2009;137(6):1124–1135.
62. Yan X, et al. Endothelial cells-targeted soluble human Delta-like 4 suppresses both physiological and pathological ocular angiogenesis. *Sci China Life Sci*. 2015;58(5):425–431.
63. Carvalho JR, et al. Non-canonical Wnt signaling regulates junctional mechanocoupling during angiogenic collective cell migration. *Elife*. 2019;8:e45853.
64. Ratheesh A, Yap AS. A bigger picture: classical cadherins and the dynamic actin cytoskeleton. *Nat Rev Mol Cell Biol*. 2012;13(10):673–679.
65. Dejana E, et al. The role of adherens junctions and VE-cadherin in the control of vascular permeability. *J Cell Sci*. 2008;121(Pt 13):2115–2122.
66. Dejana E, et al. The control of vascular integrity by endothelial cell junctions: molecular basis and pathological implications. *Dev Cell*. 2009;16(2):209–221.
67. National Genomics Data Center Members Partners. Database resources of the National Genomics Data Center in 2020. *Nucleic Acids Res*. 2020;48(D1):D24–D33.
68. Vasioukhin V, et al. Hyperproliferation and defects in epithelial polarity upon conditional ablation of alpha-catenin in skin. *Cell*. 2001;104(4):605–617.
69. Claxton S, et al. Efficient, inducible Cre-recombinase activation in vascular endothelium. *Genesis*. 2008;46(2):74–80.
70. Madisen L, et al. A robust and high-throughput Cre reporting and characterization system for the whole mouse brain. *Nat Neurosci*. 2010;13(1):133–140.
71. Harada N, et al. Intestinal polyposis in mice with a dominant stable mutation of the beta-catenin gene. *EMBO J*. 1999;18(21):5931–5942.